

ON THE IMPORTANCE OF IN-PLANE SHRINKAGE AND THROUGH-THICKNESS MOISTURE GRADIENT DURING DRYING ON COCKLING AND CURLING PHENOMENA

*P. Lipponen¹, A.-L. Erkkilä², T. Leppänen¹ and
J. Hämäläinen¹*

¹University of Kuopio, Department of Physics, P.O.Box 1627 FI-70211
Kuopio, Finland

²Metso Paper, Inc., P.O. Box 587 FI-40101 Jyväskylä, Finland

ABSTRACT

Cockling and curling are unwanted phenomena that occur already in the manufacturing process and continue through the end use of paper due to moisture content changes. This paper compares the effects of different in-plane tensions and through-thickness drying profiles during the drying process on cockling and curling by means of finite element simulations. In this study, paper is treated as a heterogeneous orthotropic elasto-plastic material. The results predict that finding the optimal way to dry paper is not straightforward; it also depends on fiber orientation structure. On the other hand, defects in the fiber orientation structure of paper can be redressed at some level by drying the paper appropriately.

Keywords: Cockling; Curling; Drying; Paper; Layered fiber orientation; Finite element analysis; Elasto-plasticity

1 INTRODUCTION

Paper goes through a significant metamorphosis between the headbox and reel, changing its state from a wet dilute suspension to a dry end product. The total magnitude of change in the dry solids content of paper approaches one hundred percentage points on a paper-making line, and the change occurring at the dryer section may exceed fifty percent. Due to its heterogeneous nature, paper exhibits non-uniform local moisture expansion behaviour, and therefore also significant cockling and curling tendencies during and after drying.

Drying-related out-of-plane deformations of paper, especially cockling and curling phenomena, have been studied for decades; see e.g. [1, 2, 3, 4]. Although a great amount of research has concentrated on studying the relationship between drying and out-of-plane deformations, the direct effect of through-thickness drying conditions on cockling and curling phenomena has remained unknown. The method presented by Lipponen *et al.* in [5, 6, 7] provides a basis for analyzing how drying and out-of-plane behaviour relate to each other.

Other factors affecting the paper cockling phenomenon have also been widely studied, and especially local inhomogeneity [8], fiber orientation [8, 9], formation [10, 11], bending stiffness [2] and temperature [2, 12] have been noted to affect cockling. However, this study concentrates purely on modelling the shared effects of in-plane tensions during drying, through-thickness drying profile (based on profiles simulated at VTT (Technical Research Centre of Finland)), and sheet fiber orientation structure (measured by Metso Paper, Inc., see Section 2). Besides these issues, the remoisturizing phenomenon (to study how harmful curling can be straightened out after the dryer section) and sensitivity analysis of some parameters are also considered.

The fiber orientation measurements underlying the modelling are described in Section 2. Section 3 presents the modelling approach. This section also includes the drying profiles and CD tensions used in simulations. The numerical implementation of the modelling approach, as well as the boundary conditions used, is discussed in Section 4. Numerical simulations performed are presented in Section 5. A sensitivity analysis on a few primary parameters is also briefly discussed in Section 5. Discussion and concluding remarks concerning the model, and the findings are provided in Section 6.

2 LAYERED FIBER ORIENTATION MEASUREMENTS

The layered fiber orientation measuring method used has been proved to be valuable tool both for the study of paper forming conditions at the wet end of a paper machine [13, 14] and for estimating the structure based cockling tendency of paper sheet [15]. Since the measuring technique is introduced only briefly in references [13, 14], in this paper the layered orientation measuring method is presented in more detail, including the latest improvements in digitizing and sheet splitting techniques.

The method employed is based on sheet splitting and image analysis of the resulting layers. Good tape stripping requires uniform and appropriate tape adhesion. Splitting quality is also affected by the pressure applied during bonding and ambient air conditions. Furthermore, the tape applied should be non-stretching. The cockling simulation approach used benefits the analysis of at least almost size A4 sheet. The equipment used for measurement in this case consists of Brother LC-9L2R 23 cm × 20 m cold laminating tape and a GBC 3500 Pro Series laminating machine, although some other tape and laminator combination might have satisfied the above requirements as well.

Samples are conditioned and the whole splitting procedure is carried out under standard atmospheric conditions ($RH = 50\% \pm 2\%$, $T = 23^{\circ}\text{C} \pm 1^{\circ}\text{C}$). The tape splitting process starts with cutting and weighing the sheet (in this case 210 mm × 210 mm in size). The tape is always bonded to the sample with the help of the laminating machine. The laminating tape is first attached to the bottom side of sample and trimmed to match the cut sample sheet, at which point a scale is tared (set to zero) with the combined weight of the tape and sample resting on it. Another piece of tape is placed on the top side of the sample, and the sample is stripped in half. The bottom side, together with the tape, is weighed to determine the mass of the removed top side. The scale is now tared again using the bottom side half. Then the tape is attached to the middle layers side of the bottom half. The bottom half is split in two, whereby the new layer from the middle of the sheet is typically directly suitable (suitable basis weight) for orientation analysis. The remaining bottom half is weighed again and then used to tare the scale. Stripping continues from the middle to the bottom side until there is only one layer left (basis weight $< 20 \text{ g/m}^2$). The same procedure is carried out on the top-side half. The resulting layers can be split further if they are too heavy, but this is needed only rarely (mainly with multilayer board samples). The splitting procedure is also illustrated in Table 1.

Samples can be digitized using either a camera or a scanner, but when the areas analyzed are as large as in this case, scanning is the easier alternative. For this research paper, digitizing was done using an UltraScan 5000 flatbed

Table 1. Paper sheet tape splitting procedure.

		<i>1st splitting</i>	<i>2nd splitting</i>	<i>3rd splitting</i>	<i>7th splitting final layers</i>
Whole sheet, 70.5 g/m ²	Bottom side 37 g/m ²	Bottom side 29.8 g/m ²	Bottom side 23.3 g/m ²	...	BS, Layer 1, 6.7 g/m ²
	Top side 33.5 g/m ²				...
				Layer 3, 3.5 g/m ²	
					Layer 4, 4.7 g/m ²
					Layer 5, 5.9 g/m ²
			Layer 6, 6.5 g/m ²		Layer 6, 6.5 g/m ²
		Layer 7, 7.2 g/m ²	Layer 7, 7.2 g/m ²		Layer 7, 7.2 g/m ²

scanner. The sample layers were placed against a black background, and a 192 mm × 192 mm area was scanned from the fiber side (in contrast to the tape side) with 30 μm/pix resolution using reflective illumination. The exact alignment of layers is important.

In analyzing scanned layer images, the aim is to detect the edges of fibers or fiber bundles and to determine their orientations. Fibers are distinguishable against a dark background as high intensity values. It is also assumed that there are no other edges than those belonging to fibers. The detection of edges is based on the computation of image gradients in every image element. The gradient of the image intensity function $f(x,y)$ at position (x,y) is represented by the vector

$$\nabla f(x,y) = \begin{bmatrix} \frac{\partial f}{\partial x} \\ \frac{\partial f}{\partial y} \end{bmatrix}. \tag{1}$$

At each image point the gradient vector points in the direction of the largest possible intensity increase, and the length of the gradient vector indicates the rate of change in that direction. Thus the magnitude (length) of gradient vector is directly related to the probability that the part of the image examined represents the edge of fiber. At the fiber edge the direction of the gradient corresponds with the direction normal to the fiber edge segment in question. For a discrete digital image, the derivatives $\frac{\partial f}{\partial x}$ and $\frac{\partial f}{\partial y}$ can be

approximated through a discrete differentiation operator. The operator uses two kernels $k_x(i,j)$ and $k_y(i,j)$ that are convolved with the original image $f(x,y)$ to calculate approximations of the horizontal and vertical derivatives:

$$\frac{\partial f(x,y)}{\partial x} \approx D_x(x,y) = (f * k_x)(x,y), \quad (2)$$

$$\frac{\partial f(x,y)}{\partial y} \approx D_y(x,y) = (f * k_y)(x,y), \quad (3)$$

where * denotes a 2-dimensional convolution operation. The coefficients of the kernels used are based on the principle of binomial filter design. This ensures that no pass-band ripples are present in the Fourier transformation [16, 17]. The separable kernels designed use layer image intensity values within a 5 pixel \times 5 pixel region around each image point to approximate the corresponding image gradient

$$k_x = \begin{bmatrix} 1 & 4 & 0 & -4 & -1 \\ 4 & 16 & 0 & -16 & -4 \\ 6 & 24 & 0 & -24 & -6 \\ 4 & 16 & 0 & -16 & -4 \\ 1 & 4 & 0 & -4 & -1 \end{bmatrix}, \quad (4)$$

$$k_y = \begin{bmatrix} 1 & 4 & 6 & 4 & 1 \\ 4 & 16 & 24 & 16 & 4 \\ 0 & 0 & 0 & 0 & 0 \\ -4 & -16 & -24 & -16 & -4 \\ -1 & -4 & -6 & -4 & -1 \end{bmatrix}. \quad (5)$$

With the digitizing resolution used this means a $150 \mu\text{m} \times 150 \mu\text{m}$ region, within which $90 \mu\text{m} \times 90 \mu\text{m}$ is pronouncedly weighted.

The magnitude $|\nabla f(x,y)|$ and direction $\theta_f(x,y)$ of gradient vectors at each local image point are calculated applying equations (6) and (7)

$$|\nabla f(x,y)| = \sqrt{D_x^2 + D_y^2}, \quad (6)$$

$$\theta_f(x,y) = \tan^{-1} \frac{D_y}{D_x}. \quad (7)$$

An orientation distribution is then computed as a weighted probability

density function of local orientations $H(\theta_H)$, where the weighting factor is gradient magnitude $|\nabla f(x,y)|$. The direction histogram is

$$H(\theta_H) = \frac{\sum_{x,y} \left(|\nabla f(x,y)| \delta_{\theta_f(x,y),\theta_H} \right)}{\sum_{x,y} |\nabla f(x,y)|}, \quad (8)$$

where $\delta_{\theta_f(x,y),\theta_H}$ is Kronecker's delta function ($\delta_{\theta_f(x,y),\theta_H} = 1$ if $\theta_f = \theta_H$ and 0 otherwise) and, $\{\theta_H, \theta_f \in X : 0 \leq \theta_H, \theta_f < 360\}$, where X is a discrete space (a space of isolated angles) and θ_H and θ_f are in degrees (rather than radians).

An example of a small layer image region together with an illustration of its local gradient magnitude is presented in Fig. 1. The image analysis algorithm presented does not try to recognize individual fibers but is based on the premise that all edges showing in a layer image are the edges of fibers or fiber bundles. These fiber edges are detected from point to point with the degree of resolution used in image acquisition. This means that long fibers give several inputs to the fiber orientation distribution while short fibers only give a few. There is thus no need for any more sophisticated weighting of fiber lengths. The influence of fiber curvature on the distribution is directly included through the point by point calculations.

Discrete fiber orientation distribution examples with one degree bins are presented in Figs. 1 and 2. The main direction of orientation (orientation angle) θ is defined as the deviation of the longer symmetry axis from machine direction. Anisotropy ξ is defined as the ratio of the distribution value of the main direction and its normal: $\xi = H(\theta)/H(\theta + 90)$. This ratio can also be calculated using a mean of distribution values around the main and the normal directions within certain interval (in this study the mean values are calculated from 10° ($\theta \pm 5^\circ$) interval). Mean values are used to reduce the effect of roughness of distribution occurring in small subareas. For out-of-plane simulations layer images are sectioned to $2 \text{ mm} \times 2 \text{ mm}$ squares, and orientation distributions and parameters are calculated for all of these small regions (Fig. 3).

3 MODELLING

Two different through-thickness dry solids content profiles and several other drying parameters were applied to measured fiber orientation structures in order to study the effect of drying on the initial cockling and curling of paper after the paper machine dryer section. For out-of-plane simulations the dryer section was subdivided into seven sections. After that there was one extra step

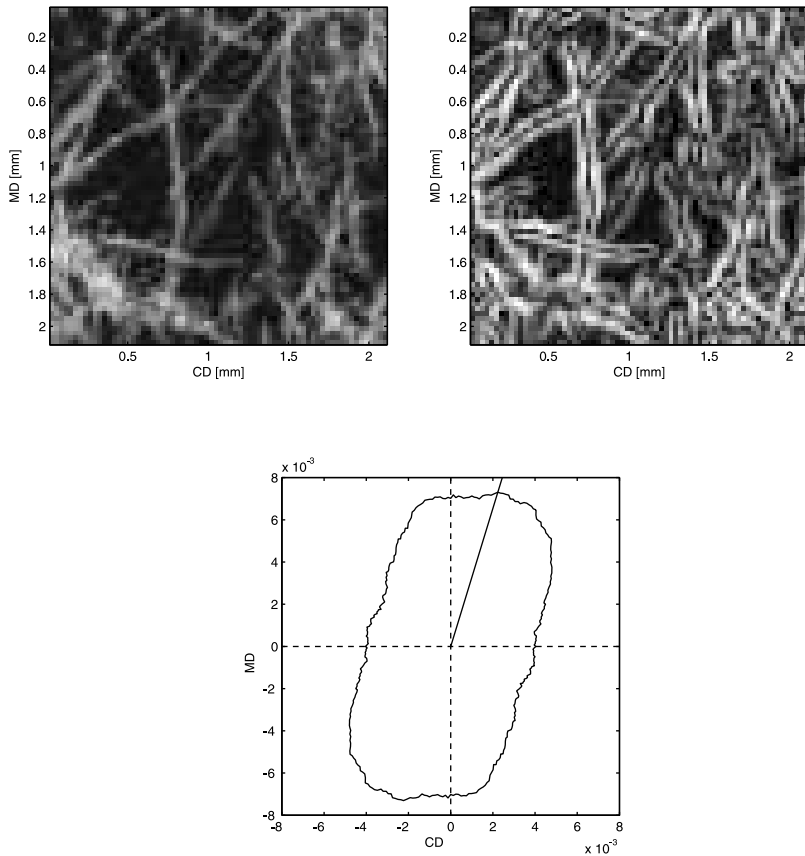


Figure 1. A small region of newsprint layer image (top left); corresponding magnitude of gradient (top right) and orientation distribution (bottom).

where external MD and CD tensions were removed (in the following this step is called drying phase 8). Fixed dry solids contents were given for different layers at each step of drying as direct inputs. Inputs were estimated using simulations of the drying model described in [18, 19]. The drying model uses such input parameters as cylinder diameter, dryer geometry, steam temperature, air humidity and temperature, etc. to calculate the sheet moisture content and drying rate along the length of the dryer section. The two through-thickness drying profiles selected for single-tier (st) and double-tier (dt) configurations are presented in Fig. 4. The simplified drying profiles used

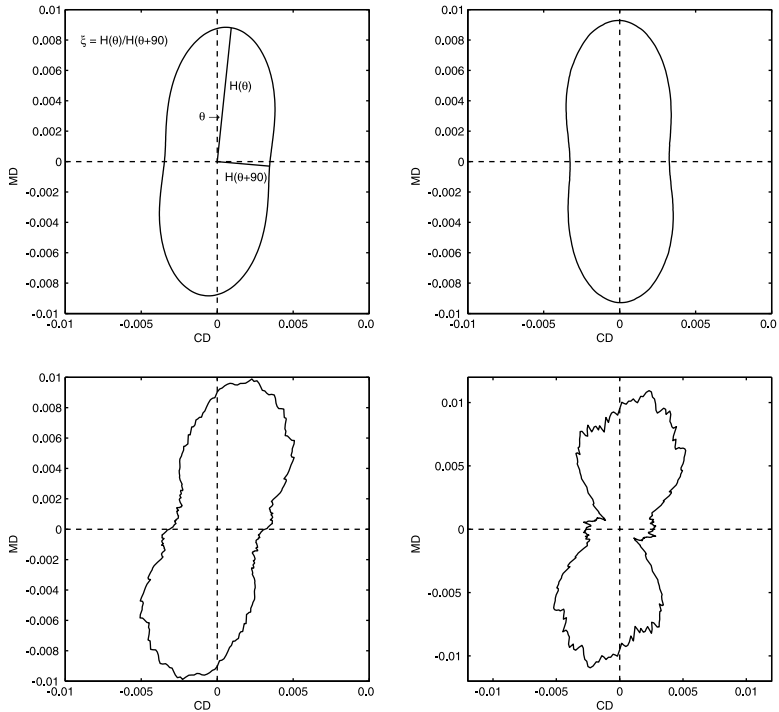


Figure 2. Examples of fiber orientation distributions calculated for areas measuring 368.64 cm² (above left), 9 cm² (above right), 0.04 cm² (below left), and 0.01 cm² (below right).

in modelling are presented in Fig. 5. These simplified profiles were obtained by first averaging layers 1, 2 and 3, which form surface 2 (st and dt), and layers 3, 4 and 5, which form surface 1 (st and dt), and then fitting a 5th degree polynomial to the averaged drying profiles. The polynomials yield the dry solids content of the paper surfaces at 7 locations along the dryer section.

To examine the effect of CD tension (together with the through-thickness drying profile), four different tension levels were studied. From the initial dry solids content to 63.9% dry solids content, CD tensions remained low due the fact that the paper web is very weak at high moisture contents and will therefore not allow high tensions at that stage [20]. After that CD shrinkage was adjusted by applying CD tensions that grew linearly to 0 N/m, 130 N/m or 260 N/m. The development of CD tension as a function of dry solids content is presented in Fig. 6. In all simulations (except the totally free drying

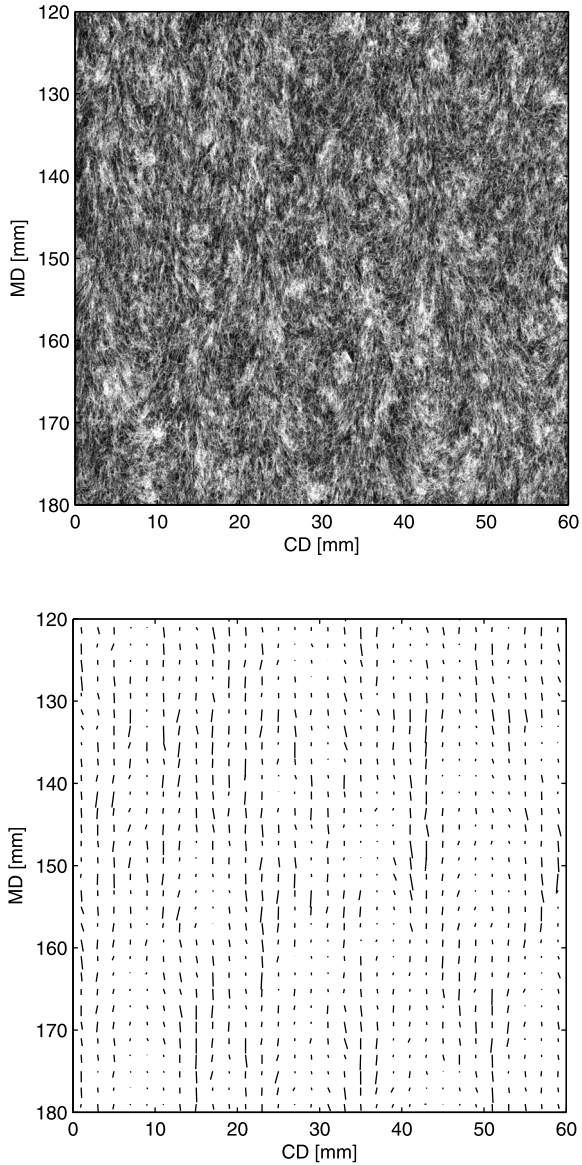


Figure 3. Example region of one layer image (top) and corresponding orientation lines (bottom) calculated for a $2\text{ mm} \times 2\text{ mm}$ subarea. The length and direction of orientation lines describe anisotropy values and orientation angles, respectively.

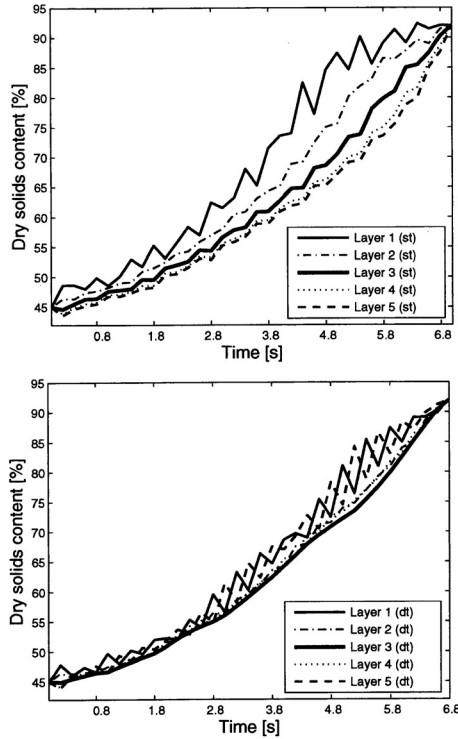


Figure 4. Simulated through-thickness drying profiles for two drying configurations. Asymmetric drying profile for a single-tier (st) drying configuration (top) and almost symmetric drying profile for a double-tier (dt) drying configuration (bottom).

case) MD tension follows CD tension, which grows to 260 N/m. The comparison of different tension levels is essential due to the fact that the paper web tends to demonstrate fairly high middle-to-edge shrinkage differences even while the total amount of shrinkage may be quite low, see e.g. [21, 22].

Although paper can be considered an elasto-visco-plastic material, the viscous nature of paper is ignored in our modelling approach. Had the viscous nature (i.e. the relaxation phenomenon in the stress-strain behaviour of paper) been included, the uncertainty of the input parameters would have increased greatly. Hence, the orthotropic elasto-plastic material model was used to investigate the effects of different drying configurations on the cockling of paper. At high enough tension levels paper crosses the border between the elastic and plastic domains and plastic (irreversible) deformation occurs.

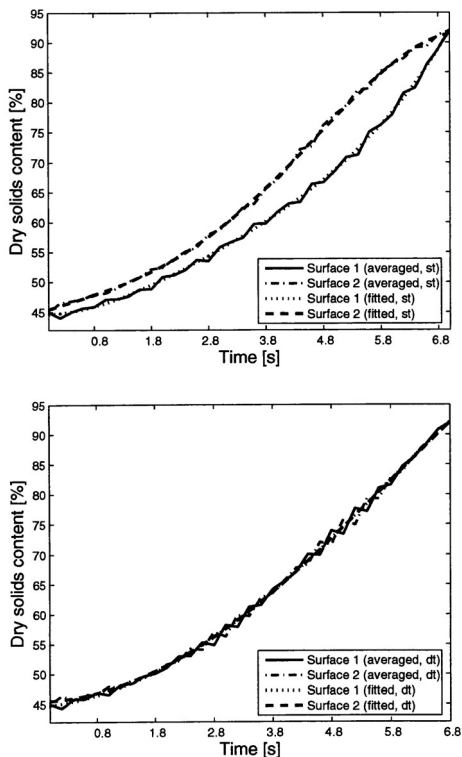


Figure 5. Simplified through-thickness drying profiles (used in modelling) for single-tier (top) and double-tier (bottom) configurations based on simulated drying profiles.

The model (which is detailed in [6]) taking into account the plastic aspects is essential when trying to capture the response from the dryer section of a paper machine. However, ignoring the viscous nature of paper affects dryer section tension levels, for example, meaning that the values obtained for the internal tension difference between the top and bottom layers of paper may increase above realistic levels. In the elasto-plastic approach used in this study, stress-strain behaviour of material is divided into elastic and plastic parts (see Fig. 7) where the yield point defines the border between the elastic and the plastic domain. The dependence used for yield stress and yield strain on dry solids content and anisotropy is based on measurements [6] and can be seen in Fig. 8 for direction 1. Direction 1 is the direction of the local fiber orientation, direction 2 runs perpendicular to that direction, and direction

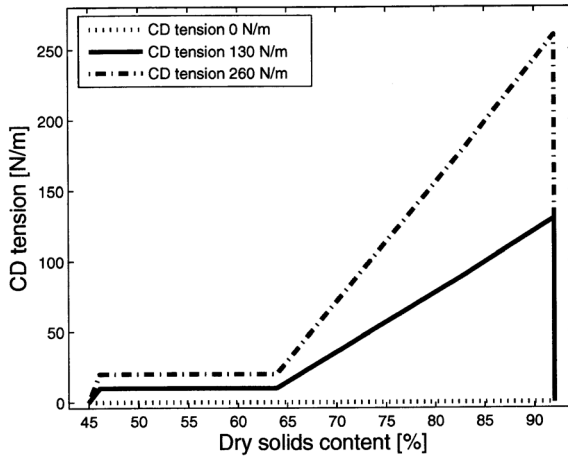


Figure 6. CD tension development to final values of 0 N/m, 130 N/m and 260 N/m for single-tier and double-tier drying configurations.

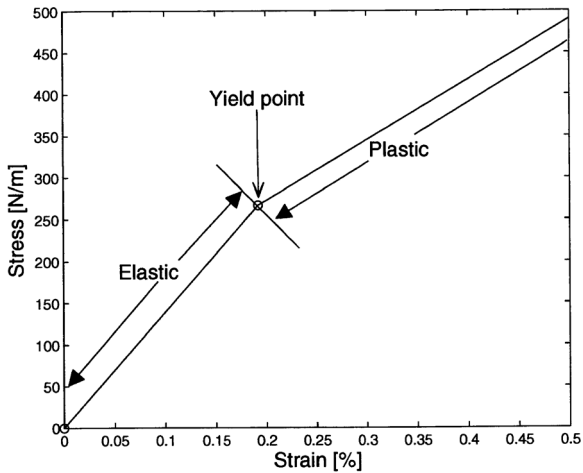


Figure 7. The yield point separates the elastic and plastic parts of materials. The yield point presented here is based on the material model used in direction 1, with anisotropy of 2 and 80% dry solids content.

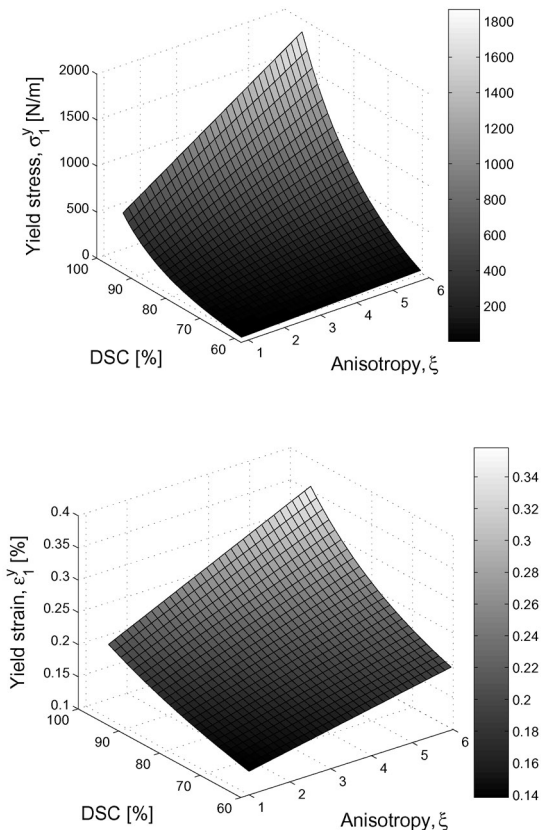


Figure 8. Example of dependence of yield stress σ^y (top) and yield strain ε^y (bottom) on anisotropy ξ and dry solids content (DSC) of paper in the elasto-plastic modelling approach in direction 1.

45° is in the middle between these directions. For more information on how local fiber orientation is treated in the model, see Section 4. The dependences of yield stress σ^y and yield strain ε^y on dry solids content β and anisotropy ξ was obtained by fitting the non-linear functions

$$\sigma^y = A_1\xi + A_2e^{A_3\beta} + A_4 + A_5\xi e^{A_6\beta}, \quad (9)$$

$$\varepsilon^y = B_1\xi + B_2e^{B_3\beta} + B_4 + B_5\xi e^{B_6\beta}, \quad (10)$$

to the measurement-based yield points. The values of coefficients A_i and B_i for all directions can be found in reference [6].

The yield surface, which determines whether yield is occurring, is defined by Hill's yield function

$$f(\boldsymbol{\sigma}) = \sqrt{F\sigma_2^2 + G\sigma_1^2 + H(\sigma_1 - \sigma_2)^2 + 2N\sigma_{12}^2}, \quad (11)$$

where parameters F , G , H and N depend on yield stresses as follows

$$H = \frac{1}{2}, \quad (12)$$

$$F = \left(\frac{\sigma_1^y}{\sigma_2^y}\right)^2 - \frac{1}{2}, \quad (13)$$

$$N = 2\left(\frac{\sigma_1^y}{\sigma_{45^\circ}^y}\right)^2 - \frac{1}{2}\left(\frac{\sigma_1^y}{\sigma_2^y}\right)^2, \quad (14)$$

when parameter H for the biaxial stress state is approximated by Hoffman's approximation ($G = H$), the suitability of which for paper is tested in [23]. Strain hardening determines the stress-strain behaviour of materials when yield occurs. The strain hardening used is defined as in reference [6].

The construction of the elastic domain used in the model is based on the determination of yield points. The elastic moduli of paper in directions 1, 2 and 45° are defined as

$$E_1 = \frac{\sigma_1^y}{\epsilon_1^y}, \quad (15)$$

$$E_2 = \frac{\sigma_2^y}{\epsilon_2^y}, \quad (16)$$

$$E_{45^\circ} = \frac{\sigma_{45^\circ}^y}{\epsilon_{45^\circ}^y}. \quad (17)$$

According to [24], shear modulus G_{12} can be approximated as

$$G_{12} = \frac{1}{\left(\frac{4}{E_{45^\circ}} - \frac{1}{E_1} - \frac{1}{E_2} + \frac{2\nu_{12}}{E_1}\right)}, \quad (18)$$

where ν_{12} is Poisson's ratio. Poisson's ratios are computed as follows

$$\nu_{12} = (1.65 - 0.015\beta)\sqrt{\xi}, \quad (19)$$

$$\nu_{21} = \frac{E_2}{E_1}\nu_{12}. \quad (20)$$

The behaviour of ν_{12} is based on experimental data presented in reference [25], and ν_{21} is simply obtained by applying a Maxwell relation. The dependence of moisture expansion coefficients on anisotropy is taken into account by quoting the work of Uesaka, see [26]. Therefore, the local moisture expansion coefficients and can be written as

$$\alpha_1 = 6 \cdot 10^{-4} - 1.5 \cdot 10^{-4} \sqrt{\xi - 1} \%^{-1}, \quad (21)$$

$$\alpha_2 = \sqrt{7 \cdot 10^{-8}(\xi - 1) + 6 \cdot 10^{-4}} \%^{-1}. \quad (22)$$

4 BOUNDARY CONDITIONS AND NUMERICAL SOLUTION

In finite element analysis paper samples are divided into 2 mm × 2 mm elements. Each element is divided into several layers in the thickness direction. Every layer of each element has its individual material parameters defined by the measured fiber orientation parameters (θ_i, ξ_i), see Fig. 9. In the

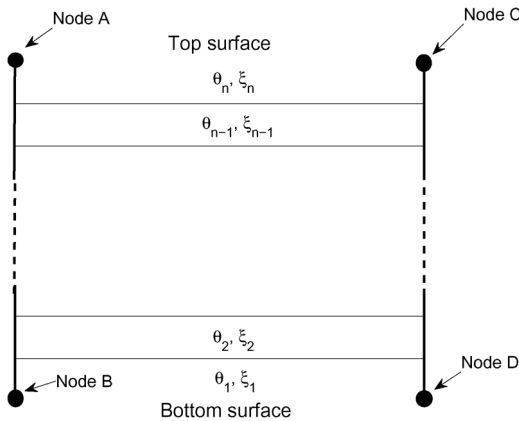


Figure 9. Cross-section of the element used in the numerical simulation. Nodes A and B form a pair, as do nodes C and D.

simulations, the tensions presented in the previous section affect the edges of the paper sheet at the dryer section. One more simulation step is carried out after the dryer section. During this step, all external tensions affecting the paper sheet are removed and displacement results are gathered.

The model is solved using ABAQUS/Standard software and element type SC8R. Element SC8R is based on first-order shear deformation theory in which the hypotheses of the classical laminated plate theory are relaxed by removing the requirement that the normal of the reference surface should remain perpendicular to the deformed reference surface. Element SC8R uses linear interpolation and reduced integration. Reduced integration means that an integration scheme one order below the full scheme is used to integrate the element's internal forces and stiffness. Reduced integration has been proven to have many advantages. For example, it could be used to avoid numerical problems and for decreasing computing time. The element used accounts for finite membrane strains and arbitrary large rotations, and it also includes the effect of thickness changes. These features make the element suitable for large-strain analysis. Unlike more commonly used shell elements, SC8R discretizes an entire 3D body. Its eight nodes are located at the corners of the top and bottom surfaces (see Fig. 9), and it has degrees of freedom only for displacements. Full details can be found in [27, 28].

Two different displacement constraints were used in the simulations depending on the phenomenon considered. The rigid body motions of the paper sheet were removed by constraining the displacements of three nodes to study curling. These nodes belong to the bottom node layer and are located in the middle of the sheet. This location allows curling fully, i.e. curling is not constrained in any direction. In one of these constrained nodes displacement is set to zero for all directions (MD, CD, z), in the second node MD and z displacement are set to zero, and in the third node only z displacement is set to zero. MD and CD displacement constraints are placed so that in-plane shrinkage between nodes is not constrained. When cockling is considered, more displacements are constrained. In addition to the nodes constrained in curling simulations, the z displacement of the bottom node layer at the sheet edges is set to zero. The displacement u_i of nodes in every pair of nodes (see Fig. 9) is also connected at the edges of the sample through the equation constraint

$$u_i^A = u_i^B, \quad (23)$$

$$u_i^C = u_i^D, \quad (24)$$

\vdots

where direction i is MD or CD depending on the sheet edge in question. If a

pair of nodes is located at the edge perpendicular to the MD, the MD displacements of the node pair are identical. The CD displacements of a pair of nodes are equal if the nodes are located at the edge perpendicular to the CD. This connection between node pair displacements removes the oscillation of stresses that appears near the edges of the sheet. This enables the use of the whole simulated area when cockling results are analyzed. Together with the z displacement constraints at the sheet edges this connection also efficiently prevents large scale out-of-plane deformations.

When the model is solved, the shear deformation capability of the element is ignored by using huge values for parameters that affect shear deformation. The effect of this approach on the solution of the model has been tested extensively. This testing has affirmed that shear deformation can be ignored when the model is solved. Numerical aspects related to the solution have in general been considered extensively *inter alia* due to the following facts:

- Automatic addition of volume-proportional damping [27, 28] is used at the final step of the simulation (when external tensions do not affect the sheet). Volume-proportional damping is accomplished by adding small viscous forces to the equilibrium equations. This stabilization helps to avoid numerical problems that may arise from local instabilities.
- Cockling is a small-scale phenomenon and full certainty of the correctness of the solution has to be obtained, i.e. the possibility of numerical error has to be eliminated.
- In the case of curling, out-of-plane deformations are large and geometrical nonlinearity plays a large role in the solution.

Fig. 10 presents the effects of the automatic addition of volume-proportional damping on the simulated cockling. The strength of damping is controlled through damping factor c which defines how strong viscous forces are used in stabilization. Smaller coefficient c values signify weaker stabilization. Image (a) shows a whole CD cross-section (from the middle of the sheet) for one cockling simulation, while (b) provides a more detailed view of the same cross-section. As can be seen, the effect of damping on the solution is minor when the damping factor is 10^{-7} or smaller. When damping factors 10^{-9} and 10^{-12} are used, the simulated cross-sections are identical. Fig. 11 shows the effect of damping on the standard deviation of the simulated cockling. Standard deviation (SD) is used to estimate the intensity of cockling. Results presented in Fig. 11 show that the SD of the simulated cockling is not affected by damping when damping factor 10^{-9} or smaller is used. In this study, the Taylor microscale [29] is used to describe the average in-plane size of cockles. It is one of the three standard turbulence length scales. It is usually calculated from an autocorrelation function of the fluctuating

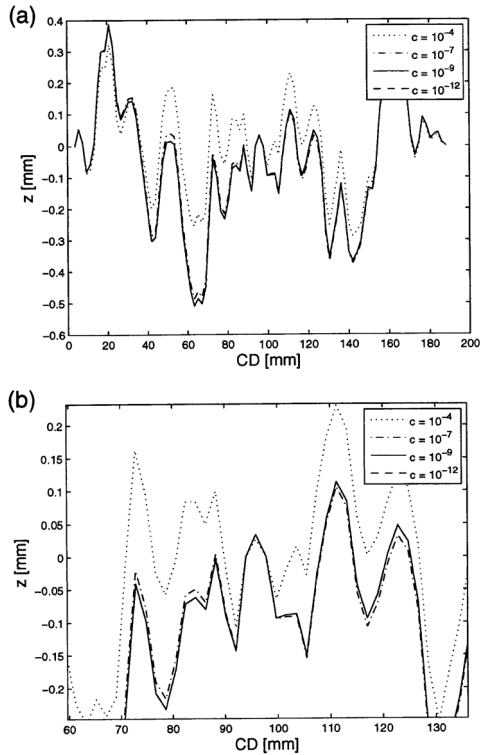


Figure 10. Effect of damping factor c on the simulated cockling. In (a), whole CD cross-section from the middle of the sheet and in (b), detail from the same cross-section.

velocity by fitting parabola (paraboloid in two-dimensional cases) around the zero-shift point at the origin and by solving the radius of the parabola. In the case of cockling, instead of fluctuating velocity, the autocorrelation is applied to the height map of cockling in spatial coordinates. The Taylor microscale is also used to characterize paper formation [29]. Fig. 12 presents how the damping factor affects MD and CD microscales. As in the case of SD, Taylor microscales are not affected by stabilization when damping factor 10^{-9} or smaller is used. Due to these observations and other numerical testing, damping factor 10^{-9} is used when cockling is considered.

Unlike cockling, curling is large-scale out-of-plane deformation. Due to this, geometrical nonlinearity plays a large role in the solution, and

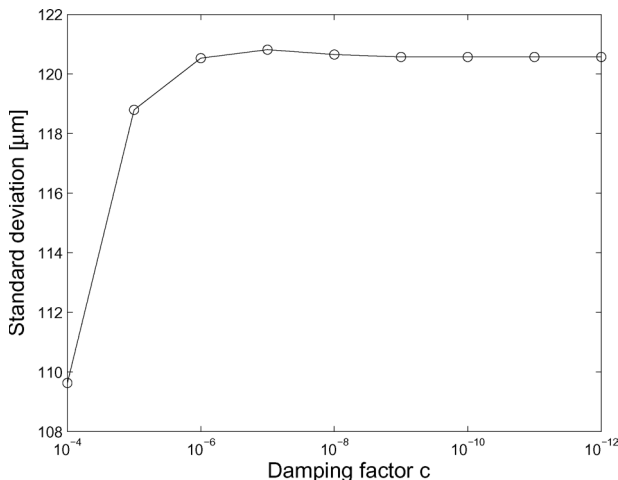


Figure 11. Standard deviation of the simulated cockling as a function of the damping factor c .

stabilization has a greater effect on the solution, see Fig. 13. Chart (a) shows a CD cross-section (from the middle of the sheet) for the simulated curling affected by non-symmetric drying. The results in (a) suggest that the damping factor does not affect the simulated curling when factor c is 10^{-11} or smaller. However, when small detail of the simulated curling presented in (a) is examined in (b), it can be seen that stabilization has a much stronger effect on the simulated curling than cockling. By comparing cases where damping factors are 10^{-14} and 10^{-15} , it can be seen that the difference between the cases is minor. Due to this and other testing, damping factor 10^{-15} is used when curling is considered.

5 RESULTS

The fiber orientation structures of ten different paper samples from ten different production machines were measured (see Section 2) to provide distinct base paper structures for drying simulations. A few examples of fiber orientation anisotropy structures through the thickness of paper from the bottom side to the top side are shown in Fig. 14. The effect of drying conditions on simulated out-of-plane deformations was studied through several simulations. The primary parameters studied were in-plane tensions during drying and the through-thickness drying profile. In the following, where cockling

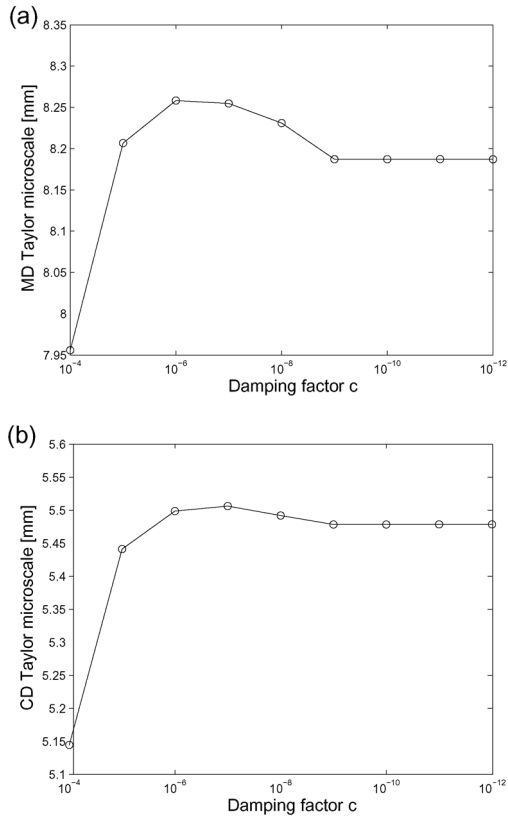


Figure 12. MD (a) and CD (b) Taylor microscales for the simulated cockling as a function of the damping factor c .

results are considered, the height map is filtered using a second-order classical IIR Butterworth filter with 50 mm cutoff wavelength. Further, where surface tensions are discussed, simulated stress is converted into N/m using the thickness of the layers employed in the simulations.

The results presented were simulated through the model introduced in the previous sections. As mentioned earlier, some of the model's inputs are measured and some are simulated by means of another model. It has to be kept in mind that the elasto-plastic approach used in the simulations requires the determination of a yield point (and whole yield surface). The quantification of the yield point and its dependence on anisotropy and the dry solids content of paper is based on the measurements presented in reference [6].

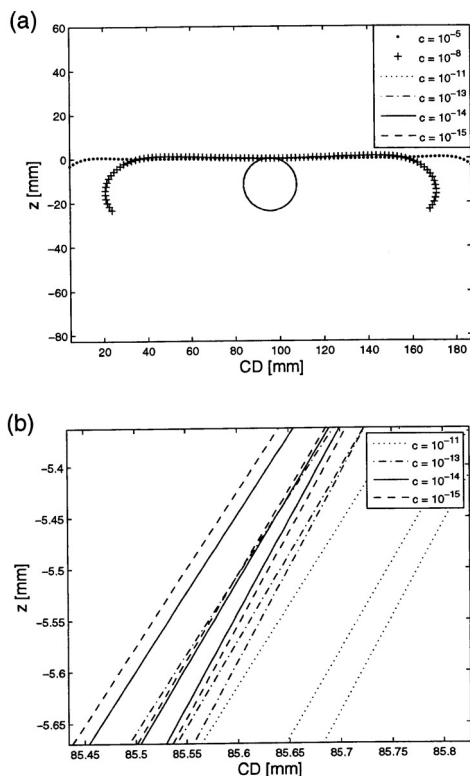


Figure 13. Effect of damping factor c on simulated curling. In (a) whole CD cross-section from the middle of the sheet and in (b) detail from the same cross-section.

However, because it is commonly known that determining the yield point is a difficult task in the case of many materials, and especially for such anisotropic materials as paper (see e.g. [30, 31, 32]), a parametric study concerning the effect of the yield point location on results is reasonable. Moreover, the effect of temperature on yield point is ignored in the model although it probably also carries its own significance as in the case of Young's modulus [33]. Fig. 15 shows two potential yield point variations. Fig. 15 shows only direction 1 yield point variation but all directions (the whole yield surface) have received similar treatment. In Fig. 15 (a) Young's modulus remains unchanged while the yield point varies, whereas in (b) Young's modulus varies while yield strain remains constant. Fig. 16 shows the effect of the variation presented in Fig. 15 (a) on simulated cockling. As can be seen in Fig. 16,

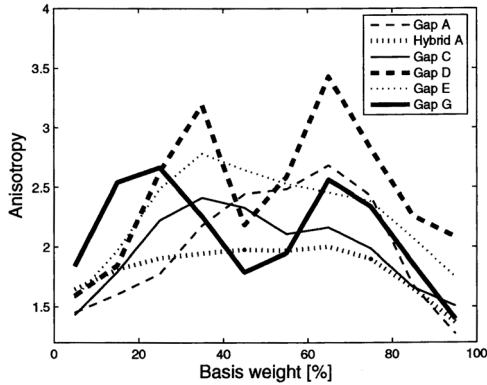


Figure 14. Fiber orientation anisotropy as a function of basis weight from bottom side to top side for different paper machine samples.

the location of the yield point has a great effect on the SD of the simulated cockling. This is quite natural, because the decrease in yield strain means that the paper enters the plastic domain earlier and more plastic deformation occurs before the release of external tensions. However, the effect seems to be very linear in nature. Meaning that the results are quite sensitive to the quantification of the yield points, but SDs still change very systematically. Therefore, when comparing the SDs of the simulated cockling of different samples, the difference between the SDs of the samples could be assumed to remain at the same level if the yield point of different samples is changed equally in the way presented in Fig. 15 (a). At the same time, the effect of a decrease in yield point on MD and CD Taylor microscapes, see Fig. 16 (in the right) is not as notable as in the case of SD of cockling.

The effect of a decrease in Young's modulus, see Fig. 15 (b), can be seen in Fig. 17. As Young's modulus decreases, so does the SD of cockling. The same effect was also noticed in the case of a decreasing yield point (with constant Young's modulus, in Fig. 16), but now the effect is less significant. That is due to the fact that now only the yield stress decreases while the yield strain remains the same. As the behaviour of the SD is very linear when moving from a decrease of 15% towards a decrease of 60%, SD suddenly drops quite considerably when a 75% decrease in Young's modulus is introduced. The steepest change in MD and CD Taylor microscapes (Fig. 17) also occurs between 60% and 75%.

In conclusion, it can be said that although determining the yield surface of paper is challenging, and it also seems to have a notable effect on the results,

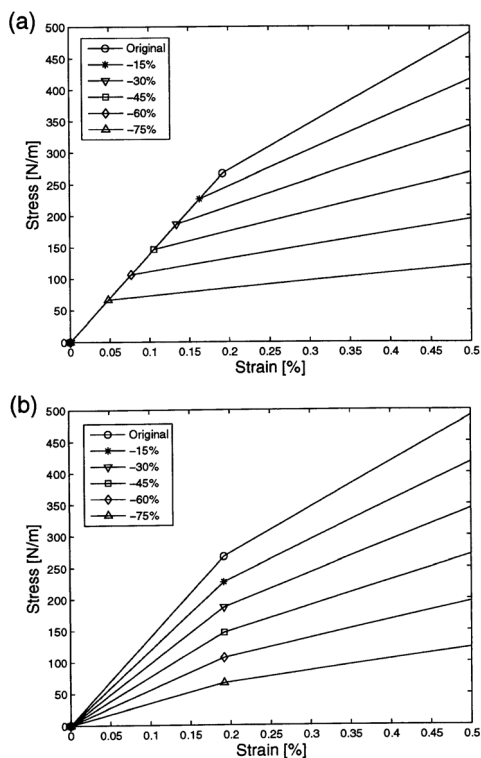


Figure 15. Example of yield point alteration (in direction 1, anisotropy 2, dry solids content 80%): in (a) decreasing yield strain and yield stress while Young's modulus remains the same, and in (b) decreasing Young's modulus while yield strain remains constant.

the effect of yield surface variations on the results is quite systematic and linear. A drop in the yield point increases plastic deformation in relation to elastic deformation. This type of a change reduces the SD of cockling, as can be observed in both of these cases.

It is widely known that through-thickness moisture gradients during the drying process represent an important factor in the curling phenomenon. Fig. 18 presents the simulated internal tension development of surfaces 1 and 2 during dt (double-tier) and st (single-tier) drying process for sample Hybrid A. As can be seen, an asymmetric drying process generates a large internal tension difference between the surfaces. In the case of a symmetric drying

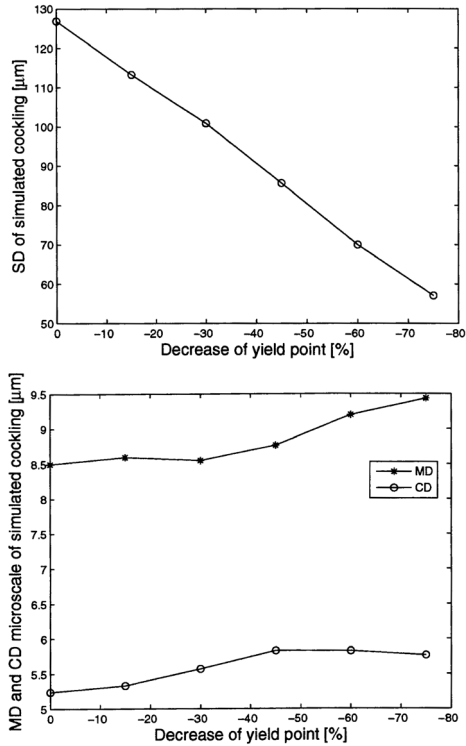


Figure 16. Effect of decreasing yield strain and yield stress on the SD of cockling and MD and CD Taylor microscale. Drying with tensions 260 N/m and 130 N/m in the MD and CD, respectively, is used in the simulations.

process, the small internal tension difference between the surfaces comes from the two-sided structure of the sample.

The internal tension difference between the surfaces strongly determines the magnitude and also the axis of curling. This can be seen in Figs. 19 and 20, where the internal tension difference between the surfaces and corresponding simulated curling in remoisturizing are presented for an almost homogeneous simplified sample. Remoisturizing is applied to a surface first dried in inverted st drying (surface 1 in Fig. 5) keeping the external tensions at drying phase 7 constant during remoisturizing. After moisture is applied to the sheet, dry solids content balance is restored at the sheet surfaces and external tensions affecting the sheet are subsequently removed. As can be seen in Fig. 19, minor remoisturizing reduces the tension difference between

the surfaces. When a certain limit is reached in remoisturizing, the tension difference between the surfaces changes its sign and the absolute value of difference starts to increase again.

Although the internal tension difference between the surfaces strongly affects the curling tendency of the sample, see Fig. 20, it alone does not define the axis of curling. When the internal tension difference between the surfaces is sufficiently low, the structure of the sample also has an effect on curling. This can be seen in Figs. 19 and 20, where 6% remoisturizing is applied to the sheet. Although the tension difference between the surfaces is higher in the MD, curling occurs around the MD axis. This stems from the fact that the sample has higher bending stiffness in the MD than CD.

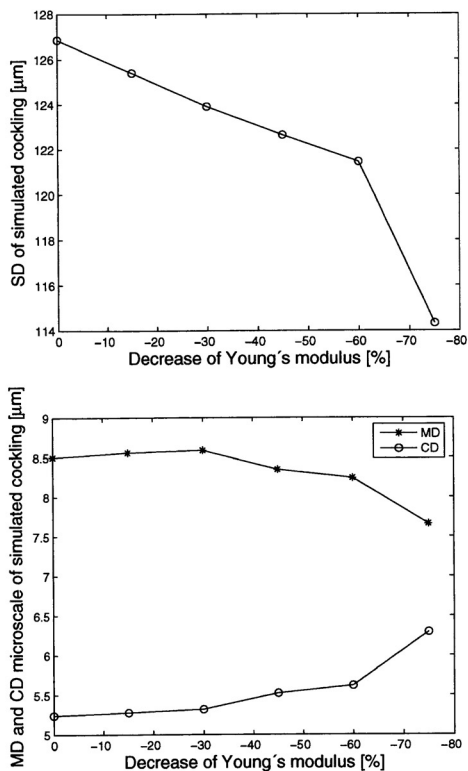


Figure 17. Effect of decreasing Young's modulus on the SD of cockling and MD and CD Taylor microscale. Dt drying with tensions 260 N/m and 130 N/m in MD and CD, respectively, is used in the simulations.

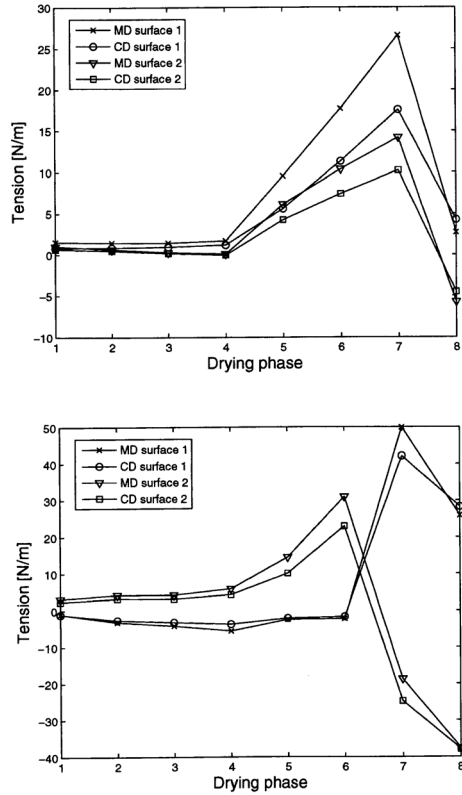


Figure 18. Internal tension (mean of surfaces) development during dt (top) and st drying (bottom) with 130 N/m CD tension for sample Hybrid A. The boundary conditions for cockling simulations are used, i.e. the sheet is not allowed to curl at drying phase 8.

Remoisturizing also affects simulated cockling. The direction of the effect of remoisturizing on cockling depends strongly on the external tensions used during the remoisturizing process. As an example, the standard deviation of simulated cockling of one sample without remoisturizing when external tensions of 260 N/m in MD and 130 N/m in CD are used is 119.0 μm . If 5% remoisturizing is applied using the same external tensions during remoisturizing as at drying phase 7, the standard deviation of simulated cockling decreases to 113.2 μm . However, if external tensions in the MD and CD are released before the remoisturizing process, the SD of cockling increases to value 126.2 μm .

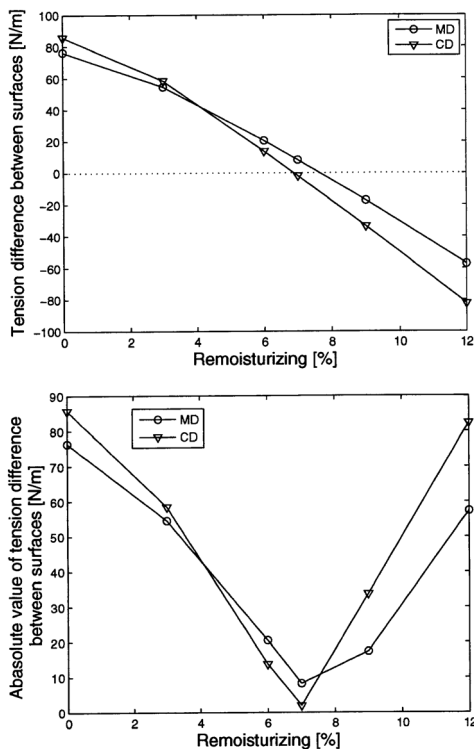


Figure 19. Internal tension difference between the surfaces before removing external tensions (top) and absolute internal tension difference between the surfaces before removing external tensions (bottom) as a function of remoisturizing for an almost homogeneous sample. The maximum values of the external tensions used are 260 N/m in the MD and 130 N/m in the CD, see Section 3. Corresponding simulated curling is presented in Fig. 20.

The local internal tension variation of the bottom and top layers for dt, st and inverted st (ID) drying with zero CD and MD external tensions during drying is presented in Fig. 21. The local tension maps simulated with boundary conditions used in the cockling studies are from drying phase 8. In inverted st drying, the drying order of the two sides of paper is changed, i.e. the surface of paper that is dried last changes. With symmetric dt drying the mean levels of internal tension are almost equal, so that the difference of mean tensions between the top and bottom layers is -6.6 N/m in the cross direction and -5.8 N/m in the machine direction. If curl were not restricted

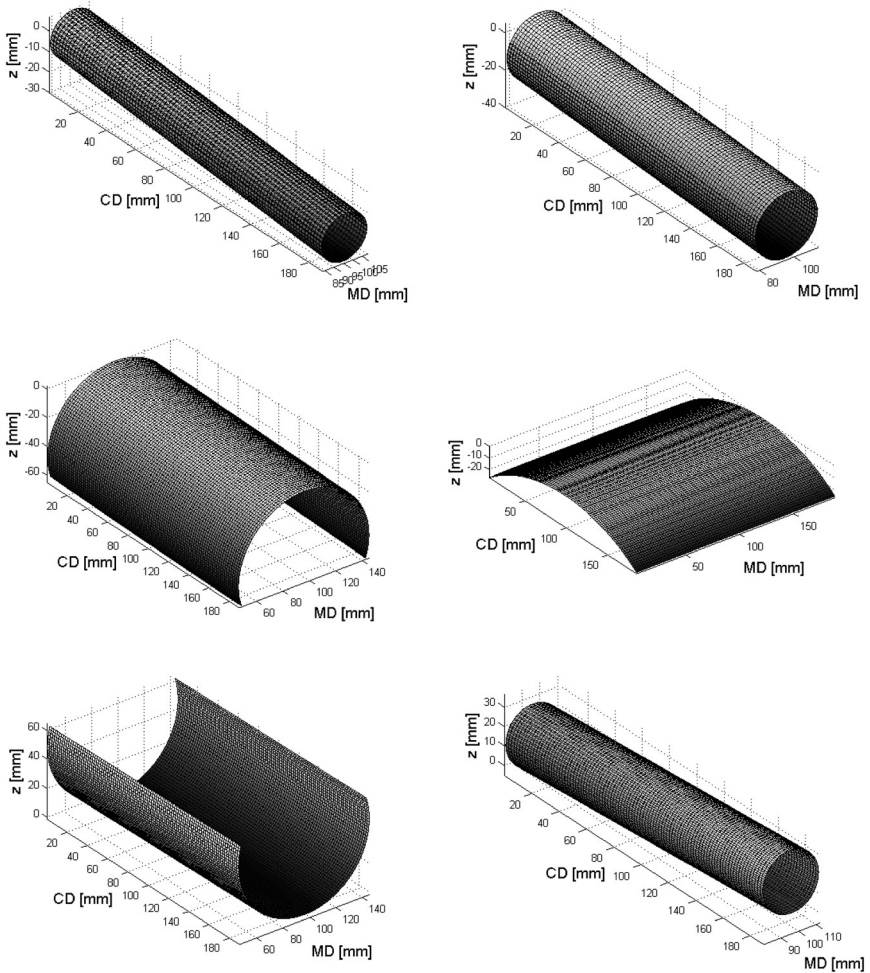
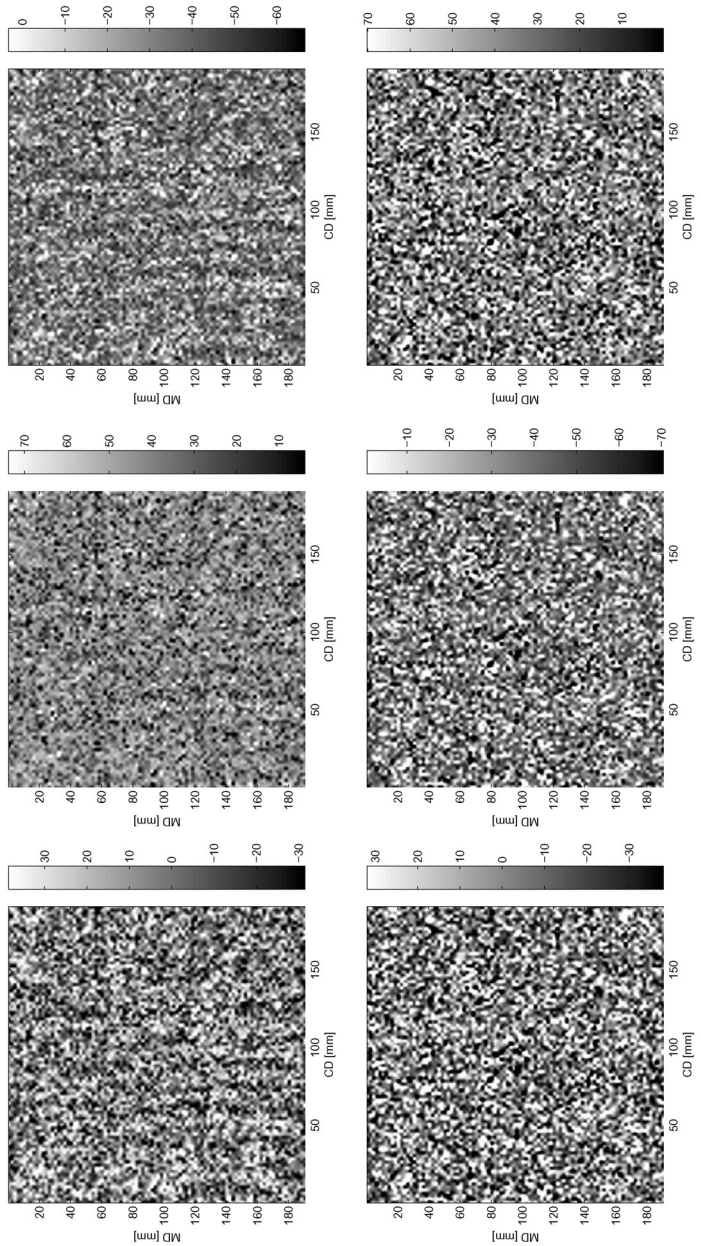


Figure 20. Simulated curling when remoisturizing 0% (top left), 3% (top right), 6% (middle left), 7% (middle right), 9% (bottom left) and 12% (bottom right) is applied to the sheet.

by means of boundary conditions, this tension difference would curl the sample so that the CD edges would rise upwards when the sample is viewed from the bottom side, i.e. the curl tendency is toward bottom side. In a non-constrained situation, i.e. this curling would minimize the internal tension two-sidedness of the sample.

The tension difference between the two sides of the sheet in symmetric drying arises directly from the anisotropy two-sidedness and elasto-plastic behaviour of its inhomogenous structure. The bottom side of the sample tends to shrink more than the top side in the CD due to the higher anisotropy of the bottom than top side layers (Fig. 14 sample Hybrid A). The anisotropy difference between the top and bottom sides is $\xi_{top30\%} - \xi_{bottom30\%} = -0.15$ (the subscript means that average values for the bottom and top sides are calculated from 30% z-direction portions of the basis weight). However, curling is prevented by the boundary conditions, which leads to a situation where the bottom side is constrained to a stretched state and top side to a compressed state in the CD. When a sample is dried in asymmetric drying (st), the tension levels of the bottom and top sides change violently (Fig. 21). In the st drying case the tension difference between the top and bottom sides increases as high as -74.3 N/m in the CD and -71.1 N/m in the MD. In this st drying the top layer (surface 2 in Fig. 5) is dried first and the bottom layer second. The result is a high curling tendency toward the bottom side. If the drying order is inverted (bottom layer is dried first), the tension differences are 66.8 N/m and 63.1 N/m in the CD and MD respectively, indicating a curling tendency toward the top side. The opposite-signed high tensions generated by two-sided dryings suppress most of the structural curling tendency arising from anisotropy two-sidedness.

The variation of bottom and top layer tensions changes only slightly when the two-sidedness of drying is inverted. Changes in the simulated cockling height maps (Fig. 21) are also minor. Only few local area alterations can be detected in out-of-plane deviations. The spectra of the cockling simulations shown in Fig. 21 are presented in Fig. 22. For this sample Hybrid A, a variance of small-scale cockling increases slightly for asymmetric drying cases and total variance is higher for the inverted st drying case than for dt and st drying. The deformation of cockling for all 10 samples measured due to different drying two-sidedness is presented in Figs. 23 and 24. The standard deviation of cockling generally increases but it can also decrease when drying two-sidedness is altered from symmetric to asymmetric. The scale of cockling oftentimes changes toward smaller cockles as the two-sidedness of drying increases. If the standard deviations of two cockling maps are equal, the visual appearance of the sample containing smaller cockles is worse. Overall, these results indicate that changes in both the nature and amplitude of cockles are minor and the directions of local curling (cockles) are mainly defined by fiber orientation two-sidedness irrespective of the drying gradient. However, small differences exist between the cockling maps, which can originate only from different ratios of elastic and plastic stresses and strains in local areas on the two sides of the sheet arising from different surface stress



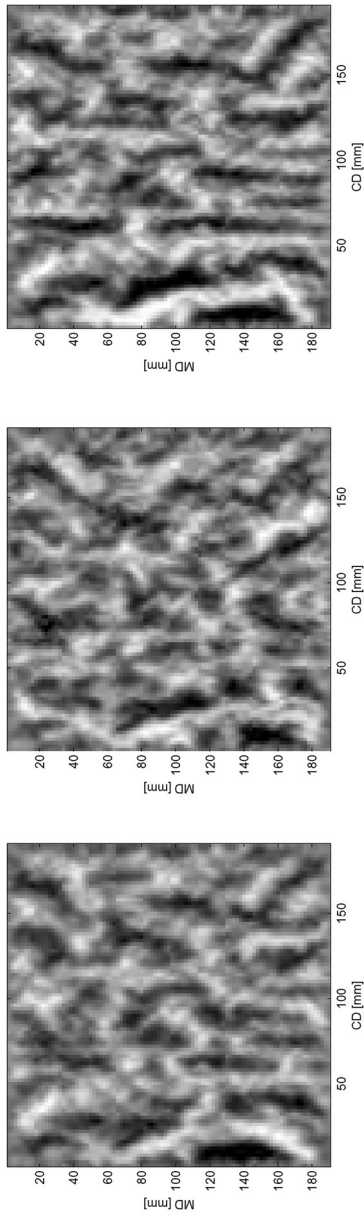


Figure 21. Local CD tensions (N/m) of bottom (top row) and top (middle row) surfaces, and corresponding cockling (bottom row) in the case of st drying (left column), st drying (middle column) and inverted st drying (right column). The vertical distance between black and white is 1 mm for all cockling figures. The sample is Hybrid A (see Fig. 14).

levels between drying arrangements (dt, st or inverted st). When these simulated cockling results are considered, suitably arranged asymmetric drying may be beneficial with certain layered orientation structures.

A small region from the bottom side CD tension map (Fig. 21) and corresponding local orientation lines for the bottom side layer and cockling of symmetric drying are presented in Fig. 25. The texture of local variations in bottom side local tension clearly correlates with corresponding height variations in the cockling image. Since local anisotropy differences constitute the only input that brings local variations to simulations, there must be some correspondence between local orientation lines and the tension map. Some correspondences can obviously be detected, but the interdependence is not straightforward. Streak-like MD structures are also seen in the tension map. High anisotropy streaks indicate negative tensions, while low anisotropy streaks correspond with positive tensions. However, in the high orientation area it would be expected that the area would tend to shrink more than the surrounding and corresponding area on the other side of the sample. If that is true, the CD tension of high orientation streaks should be positive. Simultaneously there is also a band of high anisotropy values going in the CD direction around y-axis position 130 mm. For this high orientation area tension is positive, agreeing with the presumption discussed above. High orientation streaks tend to curl locally toward the bottom side while low orientation streaks begin to curl toward the top side. A high orientation CD band tends to concurrently compress the structure not only at positions of high orientation streaks but also at positions with low orientation streaks. This means that the CD band forces the MD streaks to bend with higher amplitude waves than would be their natural tendency. In this case the CD bands can therefore explain the reversed tensions at these streak positions.

The simulation cases studied so far were dried without any constraints in the machine and cross directions. The remarkable effect of external MD and CD tensions on paper cockling is presented for sample Hybrid A in Fig. 26. The spectra in Fig. 27 show the frequency response of cockling. In the CD, the change of MD tension from free to 260 N/m during drying decreases mostly large scale variation. In the MD, a decrease in variation influences all cockling scales. If the CD tension, along with MD, is also included (0 N/m \rightarrow 130 N/m), the variations of small and middle scale cockles also decrease in the CD. No clear changes are detected in the MD. Figs. 28, 29 and 30 show how the cockling parameters of all of the samples studied depend on the CD tension used.

If drying two-sidedness is changed in a situation of restricted drying (drying tensions 260 N/m in the MD and 130 N/m in the CD), the response to this change is even lower than in the free drying case described earlier. The

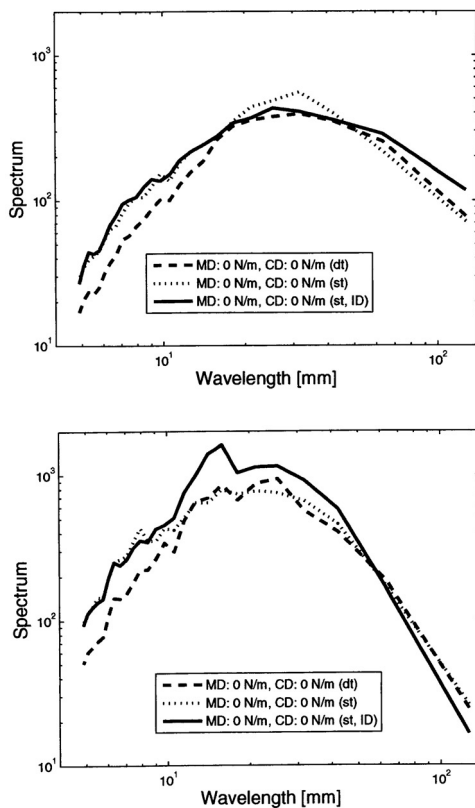


Figure 22. MD (top) and CD (bottom) spectra (from the cockling simulations shown in Fig. 21) for completely free single-tier and double-tier drying for sample Hybrid A.

cockling maps in Fig. 31 and spectra in Fig. 32 and Fig. 33 show no significant change in cockling tendency. Fig. 34 illustrates that this behaviour can be applied to all 10 production machine samples. Now, in contrast to free drying (see Fig. 23), the asymmetry of drying decreases (although only slightly) the SD of cockling in almost all cases when 260 N/m MD tension is applied. Although in st and dt drying cases the external tension introduced is equal for the same average dry solids content values (average between the top and bottom surfaces), the internal stress generated when paper dries is different in these two cases; in st drying the drier side of the paper develops higher internal stress values than either of the sides in dt drying.

With the boundary conditions used, the curl tendency of paper can be

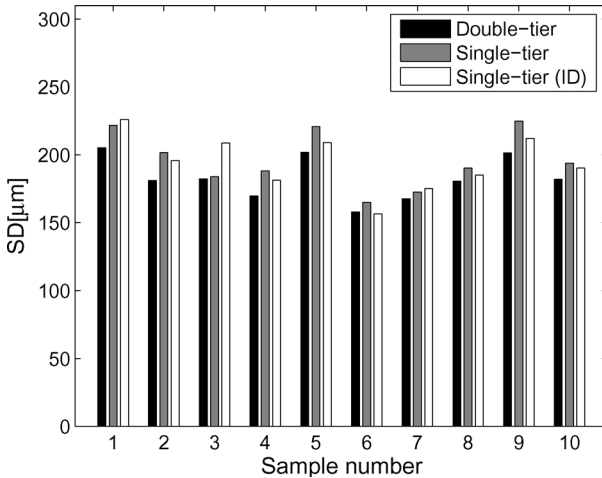


Figure 23. Standard deviation of simulated cockling in the case of completely free drying. Sample numbers 1, 2, 4, 5, 6, 8 and 9 corresponds formers gap A – G, respectively, sample number 7 correspond Fourdrinier, and sample numbers 3 and 10 corresponds hybrid A and B, respectively.

estimated on the basis of the tension difference between the two sides of the paper sheet as discussed earlier. The CD and MD tension differences of the top and bottom sides caused by different external drying tension and drying symmetry simulations are presented in Fig. 35. Symmetric dt drying shows a small negative difference in free drying and absolute value of this difference increases only slightly when drying is restricted. In symmetric drying this negative CD internal tension correlates with a negative anisotropy difference between the top and bottom sides. Both anisotropy and internal tension two-sidedness show rather low structural curl tendency for sample Hybrid A. Two-sided drying (st and inverted st) shows notably higher tension two-sidedness and thus higher curl tendency. In st drying external restrictions in the MD increases only slightly the absolute values of tension differences (CD and MD tension differences are -75.9 N/m and -73.6 N/m, respectively), and adding CD restrictions to drying lower the absolute values of internal tensions, but only slightly (CD: -66.3 N/m, MD: -63.6 N/m). In inverted st drying the internal tension difference behaves almost symmetrically when compared to st drying. Based on these simulations drying restrictions cannot reduce the extreme curl arising from two-sided drying to an acceptable level.

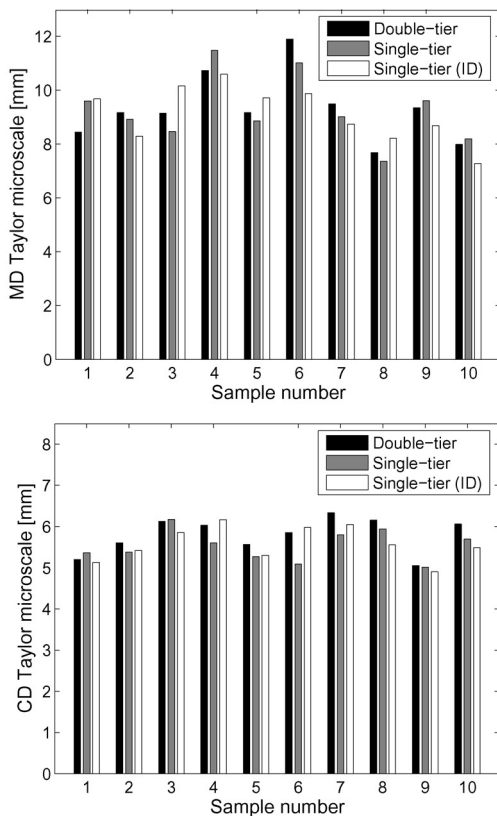


Figure 24. Taylor microscale in MD (top) and CD (bottom) in the case of completely free drying. Sample numbers 1, 2, 4, 5, 6, 8 and 9 corresponds formers gap A – G, respectively, sample number 7 correspond Fourdrinier, and sample numbers 3 and 10 corresponds hybrid A and B, respectively.

6 DISCUSSION AND CONCLUSIONS

Two different out-of-plane phenomena, the cockling and curling of paper, were examined in this study through simulations. In order to take into account the effects of the whole drying process and fiber orientation variations, an elasto-plastic material model was used despite the customary view that paper is an elasto-visco-plastic material. The viscous nature of paper means that the relaxation phenomenon in the stress-strain behaviour of the

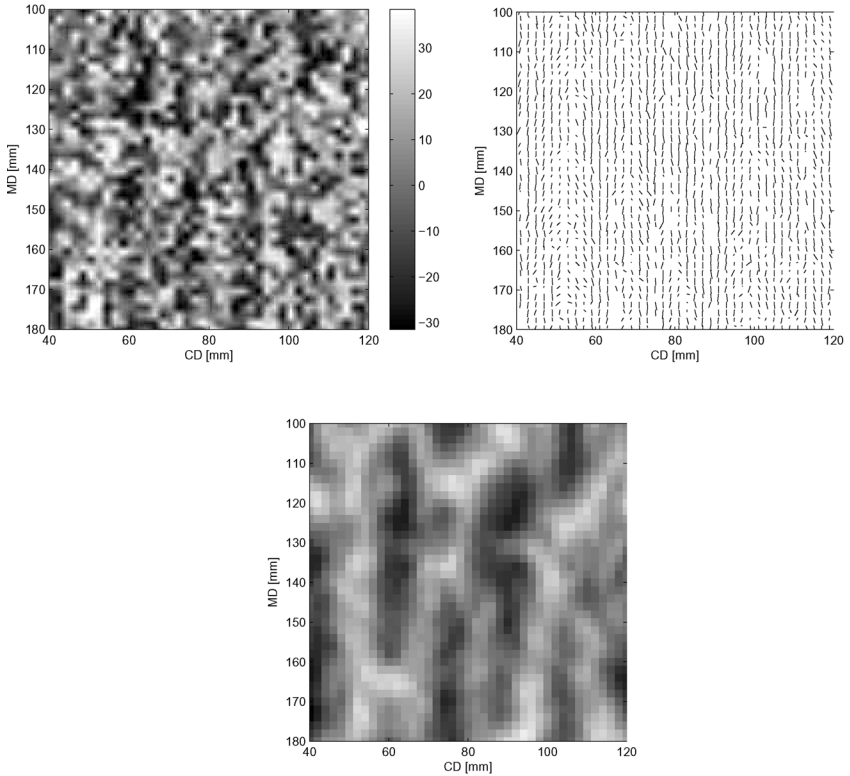


Figure 25. Small part (from sample Hybrid A) of bottom side CD tension map (top left), corresponding local orientation lines of bottom side layer (top right), and simulated cockling (bottom) when completely free dt drying is used. The vertical distance between black and white in the cockling figure is 1 mm.

sheet might also play a role in out-of-plane deformations arising at the dryer section, or at least the tensions during drying are strongly affected by relaxation. However, there is huge lack of measurement results and detailed data on the viscous phenomena taking place during the drying process. This has forced the exclusion of this viscous component from the model presented as the number of undetermined inputs would have increased to an uncontrollable level. More detailed measurement data would be needed, not only to facilitate viscous modelling but also to take full advantage of the elastoplastic model. It should also be remembered that only one structural variation, i.e. the variation of fiber orientation, is taken into account in

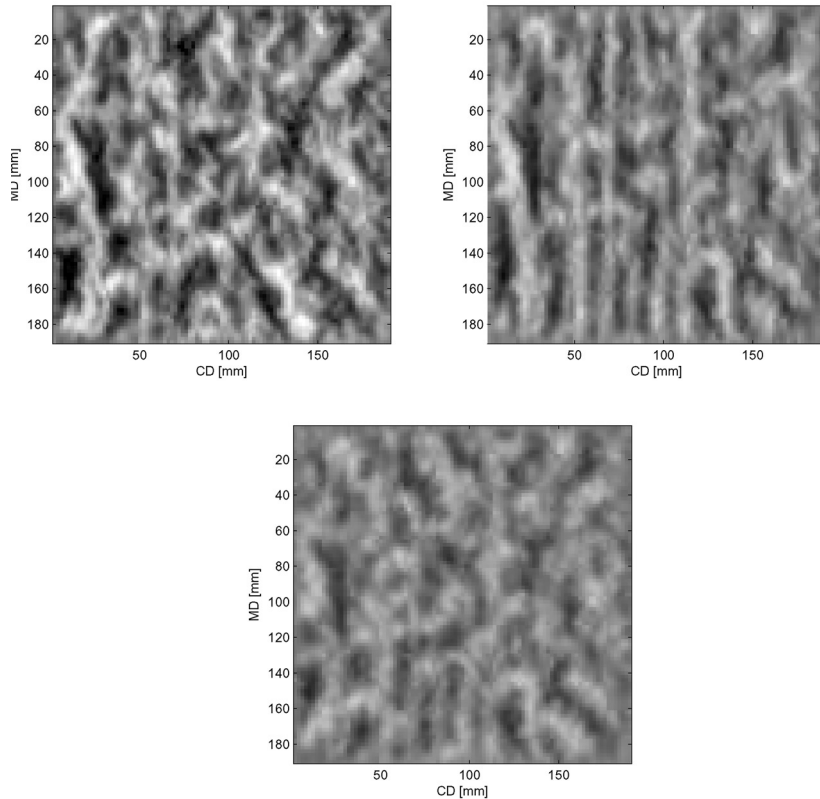


Figure 26. Simulated cockling (st drying) of sample Hybrid A in the case of completely free drying (top left), with 260 N/m MD and 0 N/m CD drying tensions (top right), and with 260 N/m MD and 130 N/m CD drying tensions (bottom). The vertical distance between black and white in the cockling figures is 1 mm.

modelling. Many other structural variations, for example in basis weight and filler content, certainly play their own important part in out-of-plane deformations. Regardless of the absence of viscous phenomena and some other detailed information of processes for inputs, the elasto-plastic model was able to produce reasonable simulation results to reveal the interactive effects of sheet structure and drying parameters on the cockling and curling of paper.

The simulation results presented in this paper indicate that the in-plane internal tensions occurring at different positions and layers of paper vary in a

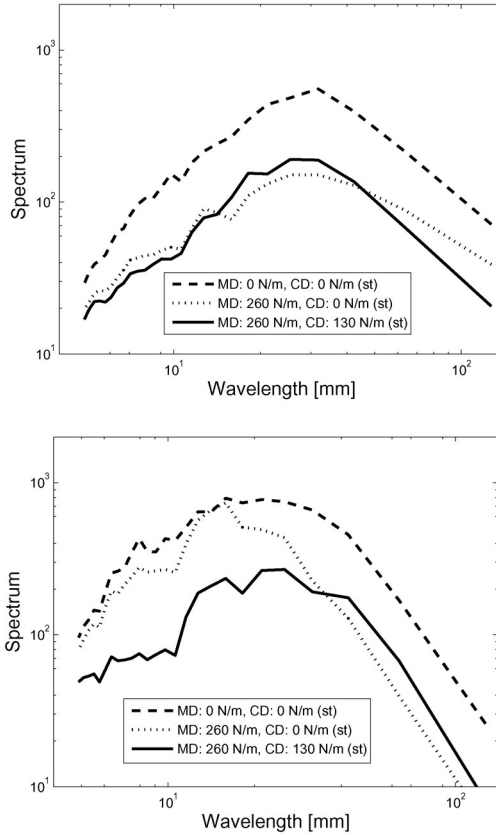


Figure 27. MD (top) and CD (bottom) spectra for single-tier drying for sample Hybrid A.

pronounced manner depending on the two-sidedness and tension conditions of drying together with the sheet’s fiber orientation structure. Drying two-sidedness is a principal factor with respect to the average internal tension levels of different paper sides, but only a minor factor in terms of tension variations within paper layers. This means that drying two-sidedness defines mainly the curling tendency of paper but has only a limited effect on cockling observed immediately after the drying process. Independently of the external MD and CD tensions used in simulation, highly asymmetric drying always leads to high two-sidedness of internal tension and thus to high curl tendency. Curling can be controlled during and after drying by adjusting this

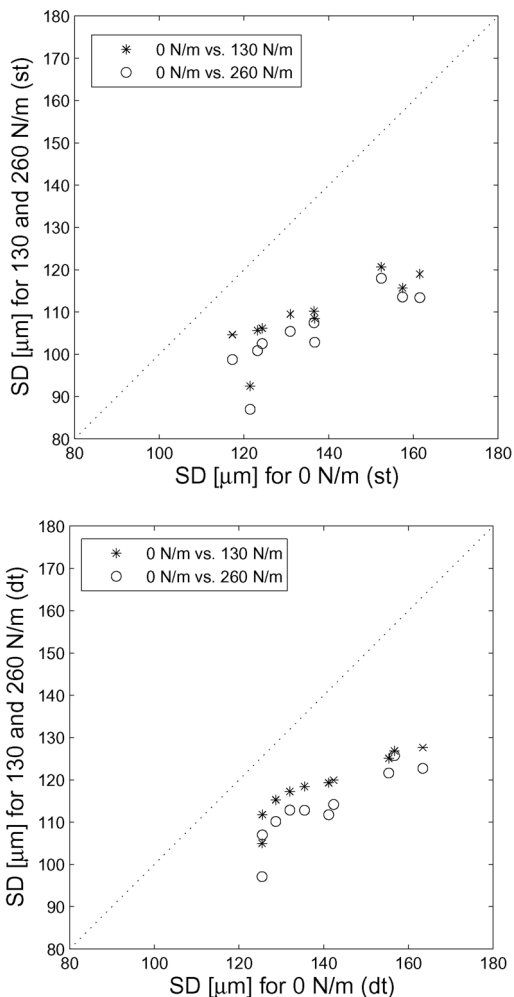


Figure 28. SD of cockling for single-tier (top) and double-tier (bottom) drying configuration in case of 0 N/m, 130 N/m and 260 N/m cross-machine tensions for ten paper samples. MD tension applied at 260 N/m. The dotted (diagonal) line is only used to facilitate comparison of the results.

internal tension two-sidedness of paper arising from drying conditions. The simulations presented in this paper show how remoisturizing and drying cycle can decrease the two-sidedness of internal tensions (and curl as well) to zero, or even force it to reverse its sign both in the MD and CD directions. This is

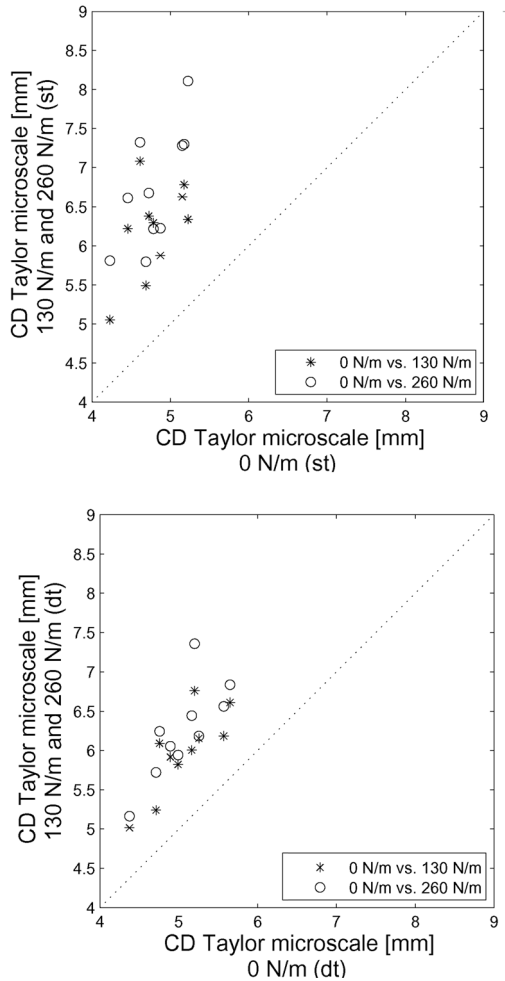


Figure 29. CD Taylor microscale of cockling for single-tier (st) and double-tier (dt) drying configurations in the case of 0 N/m, 130 N/m and 260 N/m cross-machine tensions for ten paper samples. MD tension applied at 260 N/m. The dotted (diagonal) line is only used to facilitate comparison of the results.

also true in real life: the curl tendency of asymmetric single-tier drying is always adjusted in subsequent processing of the paper web including some remoisturizing and subsequent drying or heating (e.g. remoisturizing, coating or calendering processes).

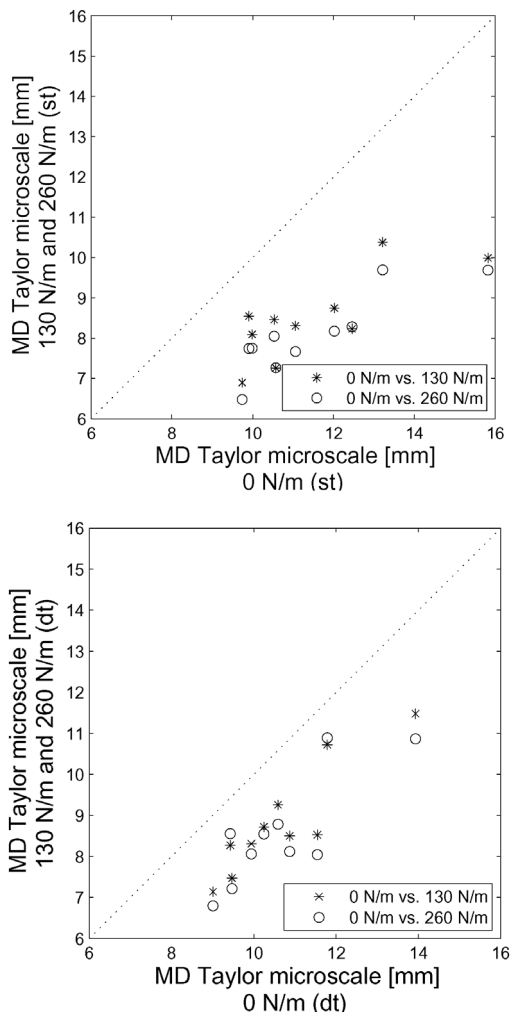


Figure 30. MD Taylor microscale of cockling for single-tier (st) and double-tier (dt) drying configurations in the case of 0 N/m, 130 N/m and 260 N/m cross-machine tensions for ten paper samples. MD tension applied at 260 N/m. The dotted (diagonal) line is only used to facilitate comparison of the results.

Based on the simulation results obtained, the asymmetry of drying has only limited ability to alter cockling tendency. Only a paper sheet with extreme two-sided variation in its fiber orientation structure can benefit from a change in the drying order of the paper surfaces. Additionally, the direction

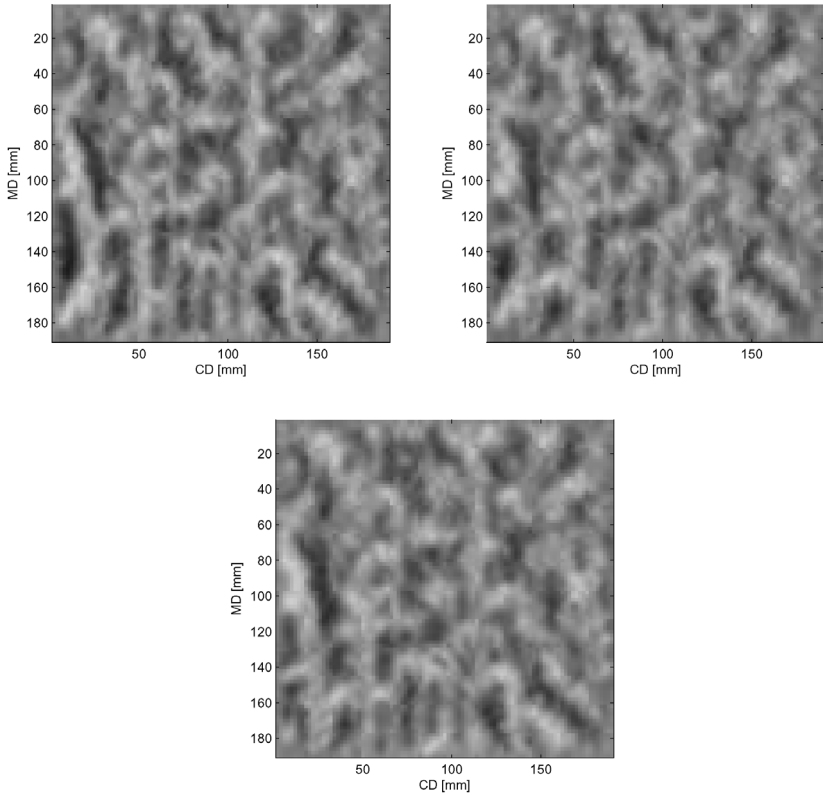


Figure 31. Cockling maps (tensions 260 N/m in the MD and 130 N/m in the CD used during drying) simulated with dt (top left), st (top right) and inverted st drying (bottom) for sample Hybrid A. Vertical distance between black and white is 1 mm for all cockling figures.

of local curls (cockles) appears to be quite stable. However, the amplitude of cockling decreases significantly if external tensions (during drying) are applied to simulated samples. The nature of cockling (such as waviness or the roundish shape of cockles) is highly influenced by the relative magnitude of MD and CD external tensions during drying, while local orientation structure defines the difference between samples taken from different production machines. The importance of drying restraints on cockling can be understood by comparing two parallel sheets, one of which is dried freely and the other totally constrained. Drying tension has to be taken into account not

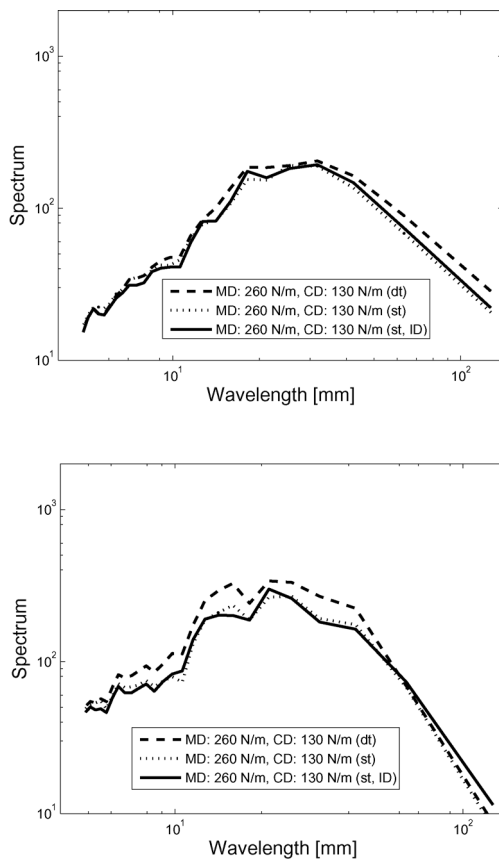


Figure 32. MD (top) and CD (bottom) spectra for dt, st and inverted st drying for sample Hybrid A with drying tensions 260 N/m and 130 N/m in the MD and CD, respectively.

only at the dryer section of a paper machine but also in the finishing, converting and conditioning of paper. If high tensions are maintained at each process stage, the risk of wasting the valuable strain potential and runnability of the paper web increases. A tension strain controlled processes might facilitate the optimization of restraints, in contrast to the straight strain (velocity) controlled drying processes typically used nowadays.

The controlling possibilities of paper machine processes concerning tensions and fiber orientation, the factors important for paper cockling, are currently inadequate. Although the profile and large-scale variations of fiber

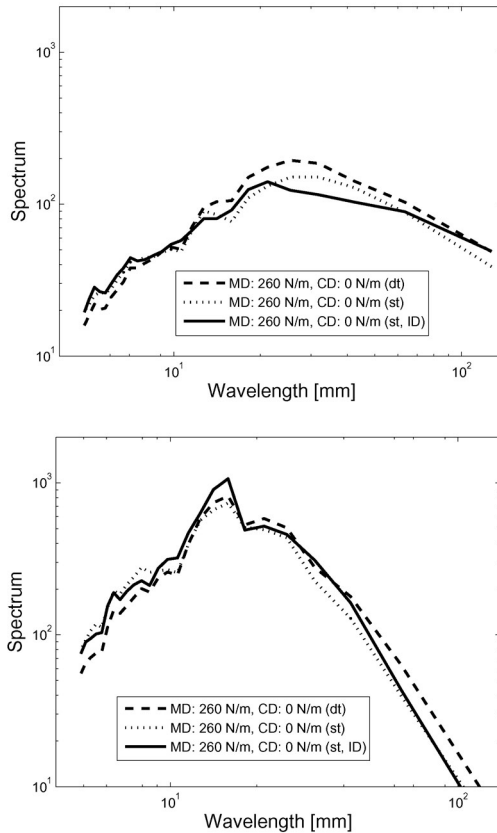


Figure 33. MD (left) and CD (right) spectra for dt, st and inverted st drying for sample Hybrid A when the CD is completely free during drying.

orientation are reasonably well controllable, controlling variations and the structure of local fiber orientation is not well understood. Precise tension levels, both MD and CD, are also impossible to adjust and control at every stage where the sheet undergoes some drying during its journey from the paper making to end use. The model presented in this paper provides a new tool for increasing general understanding of the importance of the various factors behind cockling and curl, and the simulations presented and future work with the model introduced will hopefully lead to improved process control possibilities and novel paper machine construction solutions.

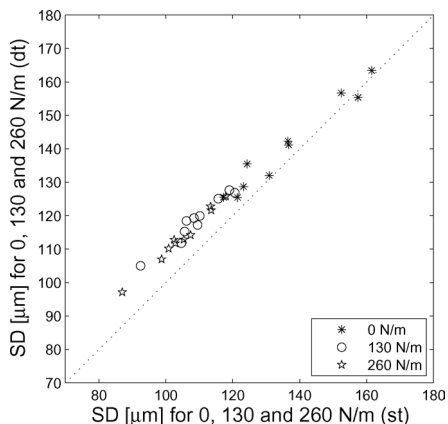


Figure 34. Comparison of the SD of cockling for single-tier (st) and double-tier (dt) drying configuration in case of 0 N/m, 130 N/m and 260 N/m cross-machine tensions for ten paper samples. MD tension applied at 260 N/m. The dotted (diagonal) line is only used to facilitate comparison of the results.

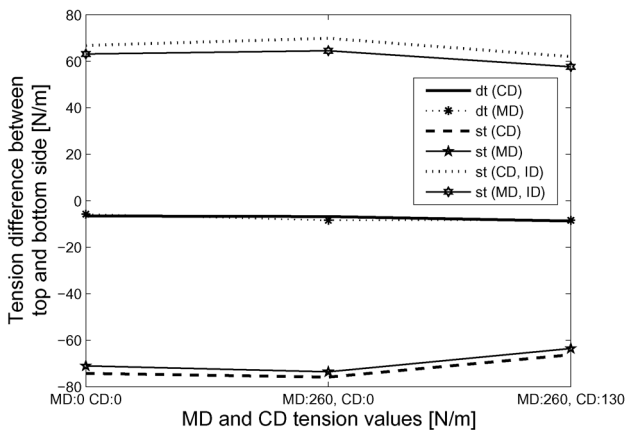


Figure 35. Internal tension difference between top and bottom sides of paper in the case of dt, st and inverted (ID) st drying for sample Hybrid A.

ACKNOWLEDGEMENTS

Special acknowledgements are due to Oleg Timofeev and Harri Kiiskinen of VTT for the through-thickness drying profiles used in this study. Special

thanks also go to Seppo Virtanen from UPM for analyzing the results and providing constructive criticism on the model, and to Heimo Ihalainen of the Tampere University of Technology for providing the signal analysis tools needed to analyze the enormous amount of data produced. The authors are grateful to UPM-Kymmene Corp. and Metso Paper, Inc. for their financial support of this research project, and for providing the experimental data used. ABAQUS/Standard, a commercial software package licensed to CSC (the Finnish IT center for science), was used to solve the model.

REFERENCES

1. Carlsson, L., Fellers, C. and Htun, M. Curl and two-sidedness of paper. *Svensk Papperstidning*, 83, 194–197, 1980.
2. Paik, K.H. and Nam, W.S. Cackle depending on drying conditions and local basis weight distribution. *J. Pulp Pap Sci.* 27, 177–181, 2001.
3. Pietikäinen, R. A mathematical model of paper sheet curling problem. Licentiate Thesis, Jyväskylä: University of Jyväskylä, 1993.
4. Smith, S.F. Dried-in strains in paper sheets and their relation to curling, cockling and other phenomena. *The Paper-Maker and British Paper Trade Journal* 119, 185–192, 1950.
5. Lipponen, P., Leppänen, T., Erkkilä, A.-L. and Hämäläinen, J. Effect of drying on simulated cockling of paper. *J. Pulp Pap Sci.* 34, 226–233, 2008.
6. Lipponen, P., Leppänen, T., Kouko, J. and Hämäläinen, J. Elasto-plastic approach for paper cockling phenomenon: On the importance of moisture gradient. *Int. J. Solids Struct.* 45, 3596–3609, 2008.
7. Lipponen, P., Leppänen, T. and Hämäläinen, J. On the role of drying induced cross-machine shrinkage on paper cockling phenomenon. *Nordic Pulp Paper Res. J.* 24, 60–65, 2009.
8. Kajanto, I. Finite element analysis of paper cockling. *Products of Papermaking*, Oxford, England, 237–262, 1993.
9. Leppänen, T., Sorvari, J., Erkkilä, A.-L. and Hämäläinen, J. Mathematical modelling of moisture induced out-of-plane deformation of a paper sheet. *Modelling Simul. Mater. Sci. Eng.* 13, 841–850, 2005.
10. Hojjatie, B. and Ahrens, F. Effects of formation and heat transfer non-uniformities on development of cackle during drying of paper. *Progress in Paper Physics Seminar*, Trondheim, Norway, 2004.
11. Ostoja-Starzewski, M. and Castro, J. Random formation, inelastic response and scale effects in paper. *Philosophical Transactions of Royal Society London A* 361, 965–986, 2003.
12. Ahrens, F., Patterson, T., Mueller, S. and Hojjatie, B. Investigation of paper dryer picking, web transfer and quality issues using a new web adhesion and drying simulator. *Brazilian J. Chem. Eng.* 22, 217–225, 2005.

13. Erkkilä, A.-L., Pakarinen, P. and Odell, M. Sheet forming studies using layered orientation analysis. *Pulp Pap. Can.* 99(1):81–85, 1998.
14. Erkkilä, A.-L., Pakarinen, P. and Odell, M. The effect of forming mechanisms on layered fiber structure in roll and blade gap forming. *TAPPI 99 – preparing for the next millennium*, TAPPI Press, Atlanta, USA, 389–400, 1999.
15. Leppänen, T., Erkkilä, A.-L., Jetsu, P. and Hämäläinen, J. Mathematical modelling of moisture induced cockling of a paper sheet. *PAPTAC 92nd Annual Meeting Preprints – Book A*, Montreal, Canada, 315–320, 2006.
16. Jähne, B. *Digital Image Processing: concepts, Algorithms and Scientific Applications*. Springer-Verlag Berlin, Heidelberg, Germany, 1991.
17. Aubury, M. and Luk, W. Binomial filters. *VLSI Signal Processing* 12(1):35–50, 1996.
18. Karlsson, M. and Timofeev, O. Computer simulation of a multicylinder dryer with single-tier configuration. *Proceedings of 5th International Symposium on Process Systems Engineering, PSE' 04*, Kyongju, 363–368, 1994.
19. Karlsson, M., Timofeev, O., Paavola, P., Malshenko, A. and Taskinen, P. Analysis of performance of multicylinder dryer, using computer simulation and experimental data. *Proceedings of the 48th Appita Annual General Conference*, Melbourne, 291–296, 1994.
20. Wedel, G.L. Restraint dryer for the drying end of a papermaking machine and a method thereof. US Patent 5933979, 1999.
21. I'Anson, S.J., Constantino, R.P.A., Hoole, S.M. and Sampson, W.W. Estimation of the Profile of Cross-Machine Shrinkage of Paper. *Measurement Sci. Technol.*, 19(1):015701, 2008.
22. Hoole, S.M., I'Anson, S.J., Ora, M., Ashworth, T.N., Briggs, D., Phillips, B. and Hoyland, R.W. CD shrinkage profiles of paper – Experiments on a commercial paper machine. *Paper Technology* 40, 63–70, 1999.
23. Suhling, J.C., Rowlands, R.E., Johnson, M.W. and Gunderson, D.E. Tensorial strength analysis of paperboard. *Experimental Mechanics* 25, 75–84, 1985.
24. Gibson, R. F. *Principles of Composite Material Mechanics*. McGraw-Hill Inc., 1994.
25. Yeh, K.C., Considine, J.M. and Suhling, J.C. The influence of moisture content on the nonlinear constitutive behavior of cellulosic materials. *Proceedings of 1991 International Paper Physics Conference*, Hawaii, USA, 695–711, 1991.
26. Uesaka, T. General formula for hygroexpansion of paper. *J. Mater. Sci.* 29, 2373–2377, 1994.
27. Hibbitt, Karlsson and Sorensen Inc., 2006. *ABAQUS Analysis User's Manual*, Version 6.6.
28. Hibbitt, Karlsson and Sorensen Inc., 2004. *ABAQUS Theory Manual*, Version 6.6.
29. Avikainen, M., Markkanen, M. and Erkkilä, A.-L. Comparison of different average floc size and scale parameters of paper formation. *Tappi Paper Physics Seminar*, Trondheim, 169–171, 2004.
30. Christensen, R. M. Observations on the definition of yield stress. *Acta Mech* 196, 239–244, 2008.

31. Htun, M. and de Ruvo, M. Correlation between the drying stresses and the internal stresses of paper. *Tappi J.* 61, 75–77, 1978.
32. Niskanen, K., 1998. *Papermaking Science and Technology, Part 16: Paper Physics*, Fapet Oy.
33. Caulfield, D. Effect of moisture and temperature on the mechanical properties of paper. *Solid mechanics advances in paper related industries: Proceedings of National Science Foundation workshop, Syracuse, NY, 50–62, 1990*

Transcription of Discussion

ON THE IMPORTANCE OF IN-PLANE SHRINKAGE AND THROUGH-THICKNESS MOISTURE GRADIENT DURING DRYING ON COCKLING AND CURLING PHENOMENA

*P. Lipponen,¹ A.-L. Erkkilä,² T. Leppänen¹ and
J. Hämäläinen¹*

¹University of Kuopio, Department of Physics, P.O.Box 1627 FI-70211,
Kuopio, Finland

²Metso Paper, Inc., P.O. Box 587 FI-40101 Jyväskylä, Finland

Tetsu Uesaka FPIInnovations

Thank you very much for your very excellent talk, it is precisely the relevant problem that we should tackle. I have one technical question. In your numerical analysis, you seem to have fixed the element size at about 2 mm × 2 mm according to the data that you have obtained from your fibre orientations, and in this case the size of the element for the numerical analysis is almost the same order of magnitude as the size of the actual structural disorder. In this case, did you actually get convergence for the solutions? Did you have any inconsistent variations in this case, particularly for cockling prediction?

Pasi Lipponen

So, what we have done is that we have tested several different sizes of the elements. Mainly done by Leppänen using the elastic model, testing element sizes of 1 mm, 2 mm, and 4 mm and no clear differences in the results

Discussion

was noticed, and we can trust that this size of element is very good in this case.

Tetsu Uesaka

When you compared the different results, did you actually compare mapping one by one for each point or did you actually take just standard deviation, or something similar.

Pasi Lipponen

Yes, standard deviation-based and visual comparison was done.

Tetsu Uesaka

Okay, so you did not compare one point to one point.

Pasi Lipponen

Yes. Point-by-point comparison was also done.

Ulrich Hirn Graz University of Technology

I have a question regarding how you gathered the material constants. Have you also incorporated different anisotropy in the fibre orientation into your model? We can assume, if you have stronger anisotropy, that the elastic constants and the yield points in the direction of fibre orientation and perpendicular to the fibre orientation are different. So have you also incorporated different elastic moduli and yield points for different levels of fibre anisotropy?

Pasi Lipponen

Yes, it has been done. The uniaxial stress–strain measurements that they made in VTT, were made using four different dry solids content levels: 65%, 75%, 85%, and 95%. The samples were tested for three different in-plane angles, MD, CD and the angle bisecting the MD and CD and moreover for three different tensile strength ratios, which were 1.5, 1.9 and 2.9.

Ulrich Hirn

These different tensile strength ratios, did they result from a variation of jet to wire speed difference, that is a variation of fibre orientation anisotropy, or was this from variations in draw or other drying conditions? You see the point I want to make is: these variations in the MD-CD ratio, do they actually come from fibre orientation changes?

Pasi Lipponen

There are anisotropy effects, yes. I do not have the function here, but it can be found in the original manuscript, but the local anisotropy is also variable in our moisture expansion coefficients, and it really affects results, if I am understanding you correctly.

Ulrich Hirn

I think so in a way, yes.

Jean-Claude Roux University of Grenoble.

In your presentation, I have some difficulty in finding where is critical moisture content. In the CD, when you have some variation of, for example, moisture content, drying cannot occur locally in the same conditions and it is a question of time. It means that the cockling phenomena can result from variation in the CD direction of the sheet of paper. So how can you deal with this critical moisture content in the sheet of paper which, according to me, is responsible for problem of cockling?

Pasi Lipponen

CD directional variation is something that we have not implemented. But what you mean by the critical value of the moisture content?

Jean-Claude Roux

You know, in the drying phenomena, you have different stages of drying. You start with some free water but as the water is more and more difficult to extract, you have difference in the profile of the dryness along the drying section. So at this level, you have change in physical phenomena and this change of physical phenomena can occur at different times or at different

Discussion

locations along the drying section. It means that some forces are applied to a local area of paper at a different time than at a different place in the CD direction. So if a part of the sheet of paper dries more quickly than its neighbours, you have different events and this can create cockling phenomena.

Pasi Lipponen

Actually, we do not have time in our model and the CD directional variation is something that we are not able to do by using this model.

Jean-Claude Roux

But probably you have a link between your yield stress and what I am talking about. It can modify the behaviour of the mechanical mechanism, elastoplastic. We can speak later.

Pasi Lipponen

Sounds good. Thank you for your comment.

Ilya Vadeiko FPIInnovations

I have a technical question about the fibre orientation that you measured in the real paper. You mentioned that you measured the edge of fibres. I was wondering if you calculated the fibre orientation distribution using individual fibres or some more statistical approach.

Pasi Lipponen

Well, each individual fibre is measured, and as a result, in this case, we get the local fibre orientation structure from 2 mm to be used in simulations. We average over the modelling element.

Ilya Vadeiko

I am asking the question because you showed on the previous slide that the resolution was about 30 μm per pixel, which is comparable roughly to a fibre width, and therefore I would imagine that it is not that easy to resolve two edges of the same fibre.

Jean-Francis Bloch University of Grenoble

The point is how you can obtain such images with 30 μm resolution. That's why we are a little bit confused here, because with a 30 μm resolution I have doubt that you can obtain such fibre orientation or images like this. You said, you used a 30 μm resolution per pixel, and the point is how can you really obtain such images with a 30 μm resolution?

Pasi Lipponen

Yes, we can obtain this distribution, but simply I cannot answer your question in detail because I really do not know; I do not have an expertise on the measurement. But those fibre orientations are real ones and there should be no reason to expect that the obtained distribution is not a real one.